The Planetary Science Journal, 3:254 (24pp), 2022 November https://doi.org/10.3847/PSJ/ac97ed

Complementary Mass Spectral Analysis of Isomeric O-bearing Organic Compounds and Fragmentation Differences through Analog Techniques for Spaceborne Mass Spectrometers

Nozair Khawaja, Jon Hillier, Fabian Klenner, Lenz Nölle, Zenghui Zou, Maryse Napoleoni, Rene Reviol, and Frank Postberg
Department of Planetary Sciences and Remote Sensing, Freie Universität Berlin, Malteser Strasse 74-100, D-12249 Berlin, Germany; nozair.khawaja@fu-berlin.de
Received 2022 July 11; revised 2022 September 28; accepted 2022 October 4; published 2022 November 11

Abstract

Mass spectrometers on board spacecraft typically use either impact ionization or electron ionization (EI) as ion sources. Understanding the similarities and differences in the spectral signatures and fragmentation patterns produced by different techniques in mass spectrometry could elucidate the composition of organic compounds. Here we present a comparison between the mass spectra obtained through laser-induced liquid beam ion desorption (LILBID; proven to simulate the impact ionization mass spectra of ice grains) and EI mass spectra of pairs of low-mass, isomeric aldehydes and ketones. Our comparison confirms that EI produces more fragmentation of carbonyl compounds, particularly aldehydes, than LILBID. We find protonated molecular ions $[M+H]^+$ in LILBID but molecular ions $[M]^+$ in EI spectra. From the evaluated species, LILBID generally produces oxygen-carrying fragment ions (e.g., $[CHO]^+$ and $[C_2H_3O]^+$) in the mass ranges 26–30 and 39–44 u, while in EI, most ions in these ranges correspond to hydrocarbon fragments. The LILBID spectra additionally show mostly protonated oxygen-bearing fragments $[CH_3O]^+$ and $[C_2H_5O]^+$ at m/z 31 and 45, less commonly observed in EI spectra. We observe a decrease in the relative intensities of cation fragment mass lines between m/z 26 and 33 and an increase between m/z 39 and 45, with an increasing carbon number for ketones and aldehydes with LILBID and EI, respectively. Our study provides a basis for complementary compositional analysis to identify the structural properties of organic species in a space environment using different spaceborne mass spectrometers (e.g., SUrface Dust Analyzer and MAss Spectrometer for Planetary EXploration) on board NASA's future Europa Clipper space mission.

Unified Astronomy Thesaurus concepts: Planetary science (1255); Europa (2189); Enceladus (2280); Mass spectrometry (2094); Astrobiology (74)

1. Introduction

Mass spectrometric analysis is extensively used in terrestrial laboratories, as well as in space, for the compositional analysis of different materials. Mass spectrometers on board a number of spacecraft have been used to study the composition of different planetary bodies by analyzing their dust environment, for example, Giotto (Kissel et al. 1986) at Halley's comet, Rosetta (Kissel et al. 2007) at comet 67/P Churyumov–Gerasimenko, and Cassini (Srama et al. 2004) in the Saturnian system (Grün et al. 2019). Recently, the detection of potential biosignatures in extraterrestrial environments in the outer solar system has become a hot topic for mass spectrometry (MS) research (Sephton et al. 2018; Klenner et al. 2020a, 2020b; Ligterink et al. 2020). Indeed, MS instruments developed for space missions (e.g., the Cosmic Dust Analyzer, CDA, on board Cassini-Huygens) have already been proven to be invaluable in detecting biologically relevant organic molecules (Postberg et al. 2018; Khawaja et al. 2019) in ice grains at Saturn.

For decades, mass spectrometers on spacecraft have utilized the phenomenon of impact ionization for MS (Dietzel et al. 1973; Grün et al. 2019) to gain insight into the compositional and dynamical properties of micron- and submicron-sized dust and ice grains in space. For this purpose, dust detectors on board spacecraft (Berg & Richardson 1969; Srama et al. 2011; Grün et al. 2019) have played an important role in characterizing the composition of interplanetary and interstellar dust and ice grains since the Pioneer 8 mission (Berg & Richardson 1969; Srama et al. 2011; Altobeli et al. 2016). In the impact ionization process (Friichtenicht 1964; Auer & Sitte 1968; Friichtenicht et al. 1971; Mocker et al. 2011), a micron- (or submicron-) sized dust grain hits the detector's solid metal target plate at hypervelocity (typically $v > 1\,\mathrm{km\,s^{-1}}$). The impinging particle partially vaporizes and creates a shock wave, which in turn produces a plasma cloud containing ions and electrons, together with neutral atoms (Friichtenicht 1964; Auer & Sitte 1968), molecules, and macroscopic fragments, with the extent of both vaporization and ionization being velocity-dependent. Electrons escape quickly from the expanding plasma due to their lower relative mass than ions, which results in a charge separation. Depending on the polarity of the instrument, an applied electric field then accelerates the chosen (positive or negative) plasma component toward an ion detector, such as a microchannel plate, generating a time-of-flight (ToF) mass spectrum (Friichtenicht 1964; Friichtenicht et al. 1971). The generated ions pass through either a field-free or a reflectron region, with lighter ions reaching the detector more quickly. In ToF impact ionization mass spectrometers, the arrival times of ions are used to calculate their mass-to-charge ratio to form a ToF mass spectrum. The type and abundance of ions from the plasma cloud are dependent on a number of factors, including impact velocity, the density of the instrument's target material, and the composition of the impacted grains. In contrast to the electron ionization (EI) MS

method, where controlled ionization of the analyte is achieved by a well-constrained electron beam, impact ionization mainly relies on the kinetic energy delivered by the impact of a grain. Therefore, ice grains with different impact speeds exhibit impact ionization mass spectra that can be quite different, even if impinging particles have the same composition.

One such impact ionization mass spectrometer, the CDA (Srama et al. 2004), on board the Cassini-Huygens space mission to Saturn, sampled ice grains (Hillier et al. 2007; Postberg et al. 2009a, 2009b, 2011, 2018; Khawaja et al. 2019) emitted from the subsurface global (Thomas et al. 2016) liquid water ocean (Iess et al. 2014) of Saturn's geologically active moon Enceladus. The in situ impact ionization mass spectra of Enceladean ice grains obtained by CDA indicated that a wide range of organic species were present in, or on, the grains (Postberg et al. 2018; Khawaja et al. 2019). In the future, another impact ionization mass spectrometer, the Surface Dust Analyzer (SUDA; Kempf et al. 2014) on NASA's Europa Clipper spacecraft, will help to explore the habitability of Jupiter's moon Europa (Howell & Pappalardo 2020) by analyzing the composition of icy grains emitted from Europa's surface or potential plumes. Similarly, for non-icy grains, the Destiny Dust Analyzer (Srama et al. 2019) on board JAXA's Destiny Plus mission will explore the composition of dust ejected from asteroid 3200 Phaethon, and the Interstellar Dust Experiment on board NASA's Interstellar Mapping and Acceleration Probe (McComas et al. 2018) will measure the elemental composition of interstellar dust.

Electrostatic accelerators are used to calibrate impact ionization mass spectrometers on Earth (Burchell et al. 1999; Mocker et al. 2011). In such accelerators, micron and submicron cosmic dust analogs, typically metallic or with a conductive coating (Hillier et al. 2009, 2012, 2014, 2018; Fielding et al. 2015), are accelerated to hypervelocities onto laboratory versions of the space-rated instruments, producing impact ionization mass spectra of the cosmic dust analogs. However, the controlled acceleration of single micrometer-sized ice grains to velocities $>5\,\mathrm{km\,s^{-1}}$ in the laboratory is currently extremely challenging (Belousov et al. 2021; Miller et al. 2022), and to simulate the impact ionization of these grains in space, an analog experiment using laser-induced liquid beam ion desorption (LILBID) is considered to be the best available technique (e.g., Klenner et al. 2019). In LILBID, a several micron thick liquid beam, the matrix, containing inorganic or organic analyte compounds is exposed to a pulsed infrared laser. Analyte compounds and the solvent matrix (e.g., water) are explosively dispersed, generating a cloud of ions (Wiederschein et al. 2015) from which ToF mass spectra of the charged species that include analyte molecules, their fragments, and corresponding water cluster species can be recorded. The LILBID instrument used for this work was first used to simulate the mass spectral features observed in Cassini CDA in situ spectra of ice grains emitted by Saturn's moon Enceladus (Postberg et al. 2009a, 2009b). Since then, a large number of organic and inorganic compounds have been measured with the LILBID facility, producing a library of mass spectral data stored in our in-house structured query language database (Klenner et al. 2022).

The most widely used laboratory MS technique is EI, in which the sample is directly exposed to a beam of high-energy electrons (approximately 70 eV) that expel electrons from neutral parent molecules, producing molecular ions $[M]^+$ with high internal energies. The structures of the molecular ions become unstable due to the generated internal energies and break up into fragment ions (Smith 2004). The EI technique is commonly used in analytical laboratories to analyze a wide range of compounds, with libraries of mass spectra available in free online databases, e.g., those of the National Institute of Standards and Technology (NIST; https://webbook.nist.gov/chemistry/), MassBank Europe (https://massbank.eu/MassBank/), and the Japanese Spectral Database for Organic Compounds (https://sdbs.db.aist.go.jp/sdbs/cgi-bin/cre_index.cgi).

In this work, we present an in-depth comparison between the mass spectral features of a selection of simple organic molecules as observed in LILBID and EI spectral data. The LILBID is regarded as a soft (Wiederschein et al. 2015) ionization technique with a focus on higher-mass spectral features (Hoffmann 2010; Klenner et al. 2020a, 2020b), whereas EI is considered to be harder (Smith 2004). In both cases, analyte molecules not only produce molecular ions but also further fragments. Our focus lies specifically on a comparative study of the cationic fragments of isomeric carbonyl compounds measured with these techniques. The compounds were selected because they produce previously identified characteristic fragment cations (Khawaja et al. 2019).

Our study provides a comparison between mass spectral features using ionization techniques employed in spacecraft-borne mass spectrometers. This work promotes the use of spectral differences of organics through LILBID and EI for elucidating the identification of unknown organic species in space environments during space missions, LILBID as an analog of impact ionization (as used by dust detectors on board different spacecraft) and EI as used in, for instance, the Ion and Neutral Mass Spectrometer on board Cassini (Waite et al. 2004) and planned for the mass spectrometers MAss Spectrometer for Planetary EXploration (MASPEX; Brockwell et al. 2016) on board the Europa Clipper mission (NASA) and PEP-NIM (Barabash et al. 2013) on board ESA's JUpiter ICy Moon Explorer spacecraft (Meyer et al. 2017). The EI mass spectrometers were also employed by past space missions, e.g., ESA's Rosetta spacecraft–carried Rosetta Orbiter Spectrometer for Ion and Neutral Analysis Double Focusing Mass Spectrometer (Balsiger et al. 2007), Cometary Sampling and Composition Experiment (Goesmann et al. 2007), and Ptolemy instrument (Morse et al. 2016) toward the comet Churyumov–Gerasimenko-67P and NASA's Curiosity Rover–carried Sample Analysis at Mars, a suite of instruments including an EI-based mass spectrometer (Mahaffy et al. 2012), toward Mars space missions. Our work has an implication to understand mass spectrometric data of space-based impact ionization and/or the EI mass spectrometers.

In general, the fragmentation behavior of an analyte molecule in one ionization method is different when compared to another technique, which generates different fragment ions and, as a result, different peak patterns in the mass spectra of the same analyte molecule. For this reason, we might not be able to exactly match the mass spectral data of the same compound obtained from two different MS techniques. The major goal of the study is to understand the similarities and differences in the composition of fragments and the spectral pattern of organics produced by LILBID and EI with an implication for spaceborne mass spectrometers, e.g., SUDA and MASPEX, which can complement each other to better understand the structural properties of organic species. It will

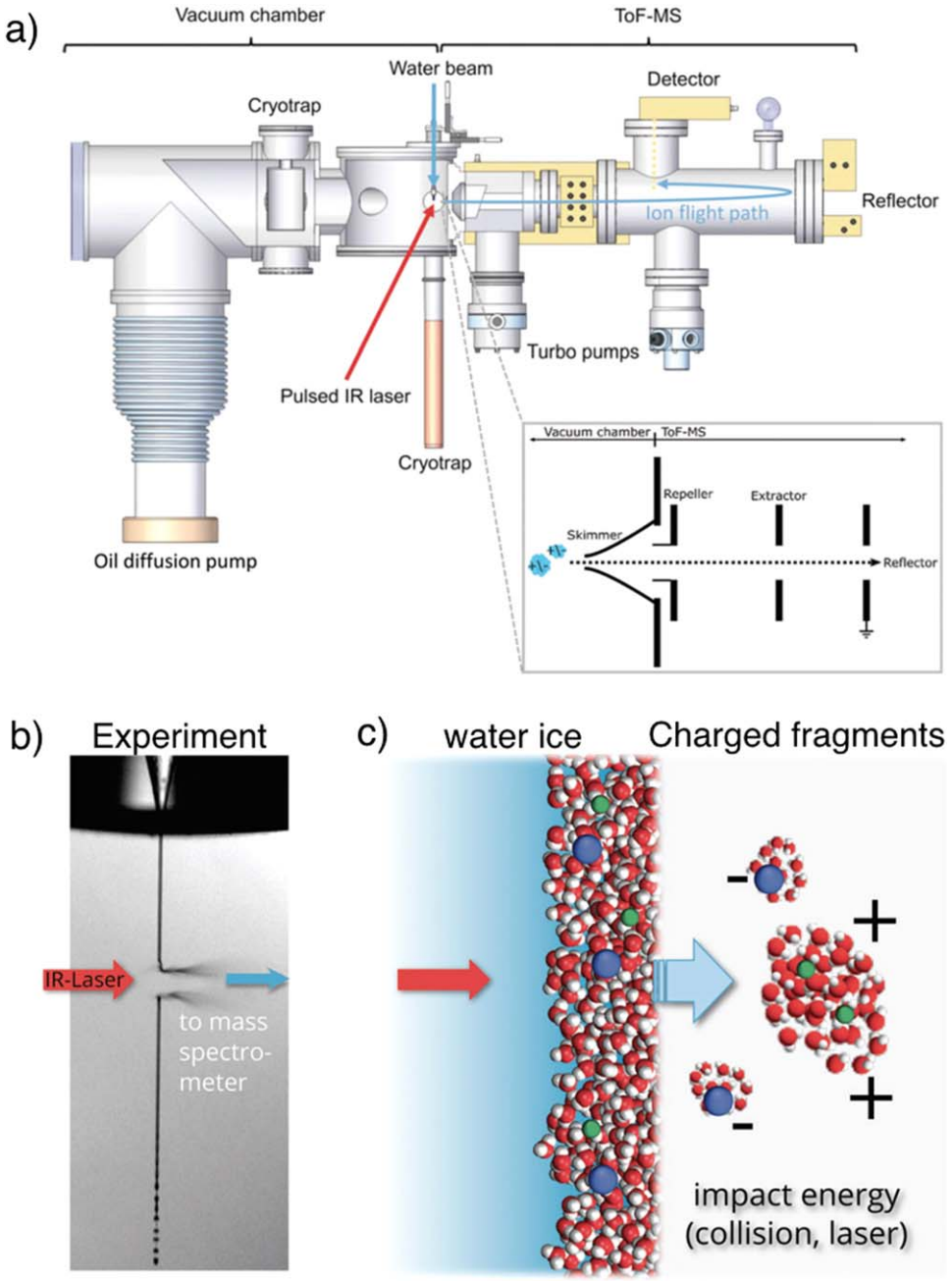

Figure 1. (a) Schematic of the LILBID-ToF-MS experiment used for this work. The schematic is taken from Klenner et al. (2019). (b) A high-speed photograph of a pulsed-IR laser irradiating a microliquid water beam in vacuum. (c) Schematic of the process (as shown in panel (b)) of a shock-wave anisotropic dispersion of a water beam into charged fragments. Panels (b) and (c) are taken and adapted from Wiederschein et al. (2015).

also enable data from existing EI spectral libraries to be applied to enhance the interpretation of in situ impact ionization mass spectral data of Enceladus's ice grains recorded by CDA in Saturn's E ring and during Enceladus's plume flybys.

2. Materials and Methods

The LILBID spectrometer was used to measure aqueous solutions of three groups of isomeric carbonyls (aldehydes and ketones), each containing compounds with three, four, or six carbon atoms. The LILBID data for these compounds were produced at the MS facility at Freie Universität Berlin (Klenner et al. 2019). The LILBID mass spectra were then compared with the corresponding EI spectral data that were retrieved from the NIST Chemistry WebBook (https://webbook.nist.gov/chemistry/).

2.1. Laser-induced Liquid Beam Ion Desorption

The LILBID facility used for this work is discussed in greater detail by Klenner et al. (2019). In the LILBID technique (Figure 1), a liquid water jet containing a dissolved analyte is vertically injected into a vacuum ($\sim 5 \times 10^{-5}$ mbar) at a constant flow rate (typically 0.20–0.25 ml minute^{-1}) through a quartz nozzle (diameter of typically 15–20 μm), where it is exposed to an adjustable pulsed infrared laser (manufacturer: OPOTEK). The laser is capable of irradiating the liquid water matrix at pulse energies of up to 4 mJ at a wavelength matching

Table 1
Isomeric Carbonyl Compounds Measured with LILBID Are Shown in Three Groups (Molecular Weight 58, 72, and 100 u) Corresponding to Three, Four, and Six Carbon Atoms in Their Molecules, Respectively

Compound	Type	Mol. Formula	Mol. Weight (u)	Supplier	Purity (%)	Concen. (mol Kg^{-1})
Propanal	Aldehyde	CH_3CH_2CHO	58	Sigma Aldrich Lot No. STBD8738V	97.0	0.05
Acetone	Ketone	CH_3COCH_3	58	abcr Lot No. 1715186	99.5	0.05
Butanal	Aldehyde	$CH_3(CH_2)_2CHO$	72	Fluka CAS No. 123-72-8	99.0	0.05
2-Butanone	Ketone	$CH_3CH_2COCH_3$	72	Sigma Aldrich Lot No. SHPF8177	99.7	0.05
Hexanal	Aldehyde	$CH_3(CH_2)_4CHO$	100	Sigma Aldrich Lot No. MKBV3600V	98.0	0.05
2-Hexanone	Ketone	$CH_3(CH_2)_3COCH_3$	100	Sigma Aldrich Lot No. MKPN7380	98.0	0.05

the OH-stretch absorption frequency of water (∼2850 nm). The water matrix (liquid beam) absorbs the laser energy in a shallow near-surface region undergoing explosive shock wave–induced anisotropic dispersion, forming charged and neutral atomic, molecular, and macroscopic fragments. The total absorbed energy remains below the combined ionization potentials and bond enthalpies of the ionized ensemble, with ion formation believed to involve the rapid dispersion of the stochastic charge distribution within the matrix (Wiederschein et al. 2015). These "mechanically" created singly charged ions (Charvat & Abel 2007) pass through a field-free drift region and are subsequently accelerated and analyzed by a reflectron (Mamyrin 1994) ToF mass spectrometer (manufacturer: Stefan Kaesdorf) with a mass resolution ($m/\Delta m$) of between ∼600 and 800.

Cations or anions, dependent on the instrument polarity, are accelerated using the principle of delayed extraction; a gating system enables the selection of ions as a function of their initial velocities using an adjustable delay time (DT) before an electric field is applied across a part of the ion cloud to accelerate ions toward the mass spectrometer. Varying the laser's power density and the DT enables the simulation of the impact ionization mass spectra of ice grains detected at different impact speeds (Klenner et al. 2019). Although the mass spectrometer is capable of measuring both polarity ions, in this work, only cation spectra were recorded to match the publicly available EI spectra.

Before initiating sample measurements, the instrument is calibrated daily using a 10^{-6} M NaCl solution at three different DT and laser intensity settings to ensure the reproducibility of spectra. For this work, six isomeric carbonyl compounds (Table 1) and one deuterated carbonyl (acetone-D6) at identical concentrations of 0.05 M in water were individually measured. To increase the signal-to-noise ratio, summed and averaged spectra were produced from 300 to 500 individual spectra per experimental setting and compound. All recorded spectra are part of a comprehensive database containing analog data for spaceborne impact ionization mass spectrometers (Klenner et al. 2022).

The resulting spectra of organic compounds may exhibit features from a range of cations. As well as from the analyte organic species, the spectra may contain mass lines corresponding to sodium (Na) and potassium (K) from trace amounts (at least below 10^{-8} M for Na and 10^{-9} M for K) of impurities left in the LILBID system from earlier measurements or from impurities in the analyte samples themselves. Although high concentrations of salts (∼0.1 M) suppress ion formation of organic molecules, the aforementioned trace amounts of alkali metal contamination do not influence the formation of organic ions in the LILBID setup (e.g., Klenner et al. 2020b). Generally, organic and inorganic cations also form water clusters that can be observed as $[\text{cation}]^+(H_2O)_{n=1-5}$ in the mass spectra (Section 2.3). Using specific DTs and laser power densities, the energy (mass) distribution of the ions produced—and subsequently detected—by the spectrometer can be altered. A comparison between spectra obtained using different experimental settings therefore provides a better understanding of fragmentation patterns and the formation of clusters (Klenner et al. 2019).

2.2. Electron Ionization

In this ionization method, an analyte is exposed to a beam of high-energy electrons (typically 70 eV). The impact of the electrons converts neutral molecules into molecular ions $[M]^+$ with higher internal energies by ejecting electrons from the orbitals of neutral molecules. Due to the absorbed energy, the structure of the $[M]^+$ becomes unstable and may fragment. In this process of breaking and forming of bonds, a substantial proportion of fragment ions of lower ionization energies (Stevenson 1951) are produced from the parent molecular ions. The product ions are often involved in a cascade of characteristic ion-forming reactions. The patterns of mass lines of these fragment ions carry structural information about the parent molecule that can be employed for the interpretation of the mass spectrum (Smith 2004).

Different types of ionization reactions occur during the EI process that result in the formation of positive (Figure 2; reactions (c), (d), (e), and (f)) and negative (Figure 2; reaction (b)) ions, as well as some neutral species in an excited state (Figure 2; reaction (a)). Without further fragmentation or ionization, the excited molecule returns to its neutral ground state, remaining undetected, and is removed by the vacuum pump. In certain instances, a very low energy electron can be absorbed into an analyte molecule to form a negative ion. However, these ions remain undetected if using an electric field arrangement and detector designed for the measurement of cations.

A cation is formed after an electron is ejected from a neutral molecule (Figure 2; reaction (c)) producing a molecular ion $[M]^+$. This ion provides information about the original parent molecule of the same mass. In further dissociation reactions (Figure 2; reactions (d) and (e)), the molecular ion is fragmented by the cleavage of a single bond, with the loss of a neutral fragment and further electrons. This process triggers the expulsion of fragments containing an even number of electrons. If more than one electron is ejected from the analyte

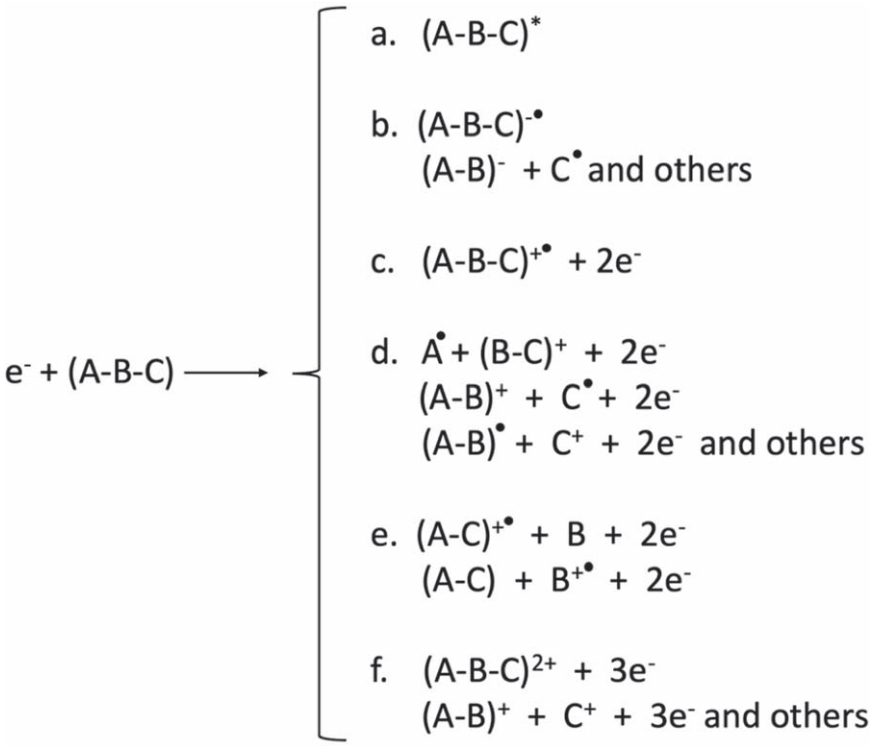

Figure 2. Different types of ionization reactions during the EI process (adapted from Smith 2004). The left side represents a molecule (A-B-C) exposed to an electron (e^-) beam of 70 eV, and the right side shows the production of different ionic and neutral species. (a) Excitation of a molecule that remains undetected, (b) formation of negative ions not detected by positive EI MS, (c) formation of a positive molecular ion, (d) formation of fragment cations, (e) formation of fragment cations with rearrangements, and (f) multiple ionization processes to form singly and doubly charged ionic species.

molecule, this leads to reaction (f) as shown in Figure 2. However, these kinds of multiply charged species are less likely to form than singly charged ion species in the EI process (Smith 2004).

2.3. Data Sets and Selection Criteria

To obtain the LILBID spectra of aldehydes (propanal, butanal, and hexanal) and ketones (acetone, 2-butanone, 2-hexanone, and deuterated acetone), an aqueous solution of each compound was measured in the laboratory at a concentration of 0.05 molar. Spectra of each compound were recorded at three different DT settings: (i) $\approx 4.5 \pm 0.3$, (ii) $\approx 5.5 \pm 0.4$, and (iii) $\approx 7.1 \pm 0.6$ μs. Different DT windows change the sensitivity of the detector to ions within specific mass ranges in which ions can be detected at high abundances. (i) The lowest DT allows fragment cations approximately up to m/z 74 to be extracted. (ii) The intermediate DT window extracts fragment cations approximately between m/z 75 and 100, whereas (iii) the highest DT window allows fragments of $m/z \geqslant 100$ to be detected at relatively high abundances.

In this study, we compare only the organic features observed in LILBID spectra (Section 3) of the selected compounds (Appendix Tables A1 and A2) with their corresponding EI spectra and therefore have excluded all spectral peaks produced by water clustering (Appendix Figures A1–A3) only from the LILBID spectra. As previously mentioned, water clusters may be isobaric (at the resolution of the spectrometer) with some organic fragment peaks (Appendix Table A3). Therefore, the removal of mass lines corresponding to water clusters may also result in the inadvertent removal of purely organic fragment cations from LILBID spectra. The different types of water clusters typically requiring removal are $([H_3O]^+(H_2O)_{n=0,1,2...})$, $([Na]^+(H_2O)_{n=0,1,2...})$, $([K]^+(H_2O)_{n=0,1,2...})$, and $([C_{1,2}H_{3,5}O]^+(H_2O)_{n=1,2...}$, $[M\text{-}OH]^+(H_2O)_{n=1,2}$, $[M+H_{1,2}]^+(H_2O)_{n=1,2...})$, where "M" refers to the molecular formula of the measured organic compound.

To consider all possible organic cationic species, the LILBID spectra of all three DTs for each compound were combined while excluding the water cluster features mentioned above. From each spectrum at a specific DT, a subsection of the mass range in which the highest abundances of fragment cations were observed was selected. From the low, intermediate, and high DT spectra of each compound, segments of spectra in each DT with m/z less than 74, between 75 and 100, and greater than 100, respectively, were selected and combined to produce a single representative spectrum for each compound. To remove spurious spectral peaks (instrument noise, infrequent mass lines), a relative intensity threshold of 0.003 was applied to the LILBID spectra prior to combining these three DT spectra (Appendix Tables A1 and A2). The LILBID spectra were then compared with the corresponding EI spectra obtained from the NIST WebBook. Here we have normalized the LILBID spectra to the amplitude of the highest peak in each spectrum similar to EI spectra (Figures 4, 6, and 8). Additionally, the LILBID spectra of all DTs of each compound were also coadded without removing any water cluster features as a reference (Appendix Figures A1–A3).

3. Results and Discussion

The three groups of investigated isomeric carbonyl compounds are shown in Table 1. The LILBID and EI spectra of these compounds show fragment cations characteristic of

carbonyl compounds. Water cluster features (Figures A1–A3) were removed prior to reconstructing the LILBID mass spectrum of each organic compound (Figures 3, 4, 6, and 8).

3.1. Carbon-3 Compounds

The LILBID and EI mass spectra of acetone and propanal, each of which possesses one oxygen, three carbon, and six hydrogen atoms, are shown in Figures 3 and 5.

In the case of acetone, the amplitudes of both spectra (Figure 3(a)) are normalized to that of the base peak at m/z 43. The molecular structure of acetone favors the cleavage of a C–C bond with the subsequent elimination of CH_3 from the parent molecule, forming $[C_2H_3O]^+$ at m/z 43 (Figure 5(a)). The cleaved CH_3 is not present in the LILBID spectrum, with it probably remaining neutrally charged given the lack of any suitable water cluster peaks, whereas in the EI spectrum, it is present at m/z 15. Another significant fragment in the LILBID spectrum appears at m/z 31, but this is absent in the EI spectrum, which instead indicates a number of minor mass lines around m/z 27, representing hydrocarbon species. The presence of a mass line at m/z 31 in the LILBID spectrum indicates cleavage of C–C bonds on both sides of the carbonyl-carbon. As a result, the oxygen-carrying protonated fragment cation in the LILBID spectrum appears at m/z 31 as $[CH_3O]^+$. We exclude the possibility of neutral carbon clustering with hydronium $[H_3O]^+C$ at m/z 31 because releasing neutral or charged elemental carbon from carbonyl compounds requires higher energy densities than those used here (Klenner et al. 2019), with the peak at m/z 31 still present in other experiments at lower energy densities (Khawaja et al. 2019). The absence of hydrocarbon clusters at m/z 32, 33, and 34 ($[H_3O]^+CH$, $[H_3O]^+CH_2$, and $[H_3O]^+CH_3$) also rules out the possibility of the release of neutral carbon and related hydrocarbons (CH, CH_2, and CH_3).

There is no clear evidence of significant clustering between neutral organic species and $[H_3O]^+$ in these LILBID spectra. However, there are a few notable exceptions, such as a 60 u (unified atomic mass unit) peak that, although it might indicate a water cluster with a deprotonated fragment cation $[C_2H_3O\text{-}H]^+(H_2O)$, could also be due to clustering of a

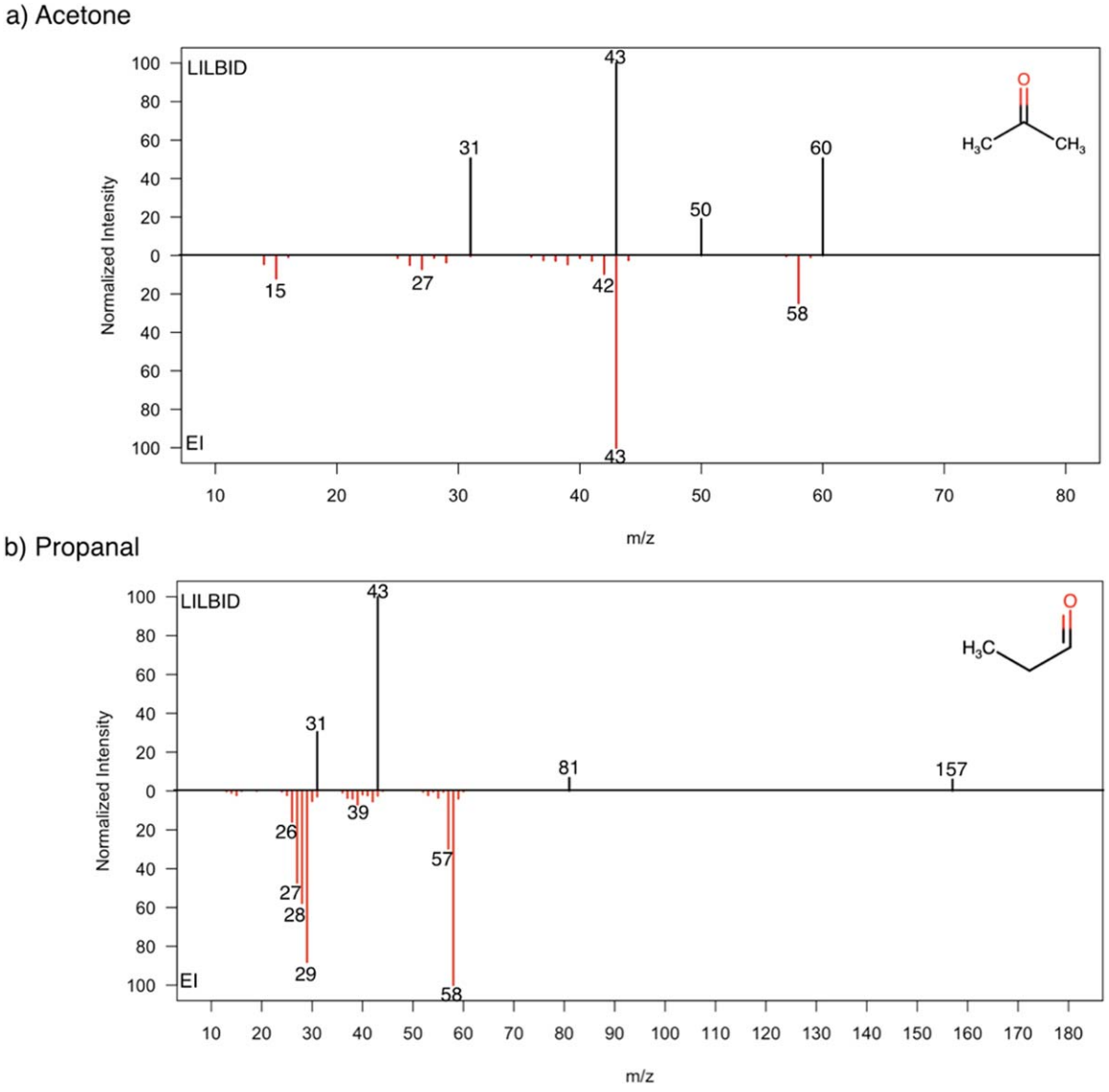

Figure 3. Mirror plots of carbon-3 isomeric carbonyl spectra produced by LILBID (top) and EI (bottom). Panel (a) shows a LILBID acetone spectrum and the corresponding spectrum from EI. Panel (b) shows a mirror plot of propanal (isomeric carbonyl of acetone). The x-axis represents m/z values, and the y-axis shows normalized relative intensity (arbitrary units). For full LILBID spectra of acetone and propanal, see Appendix Figure A1.

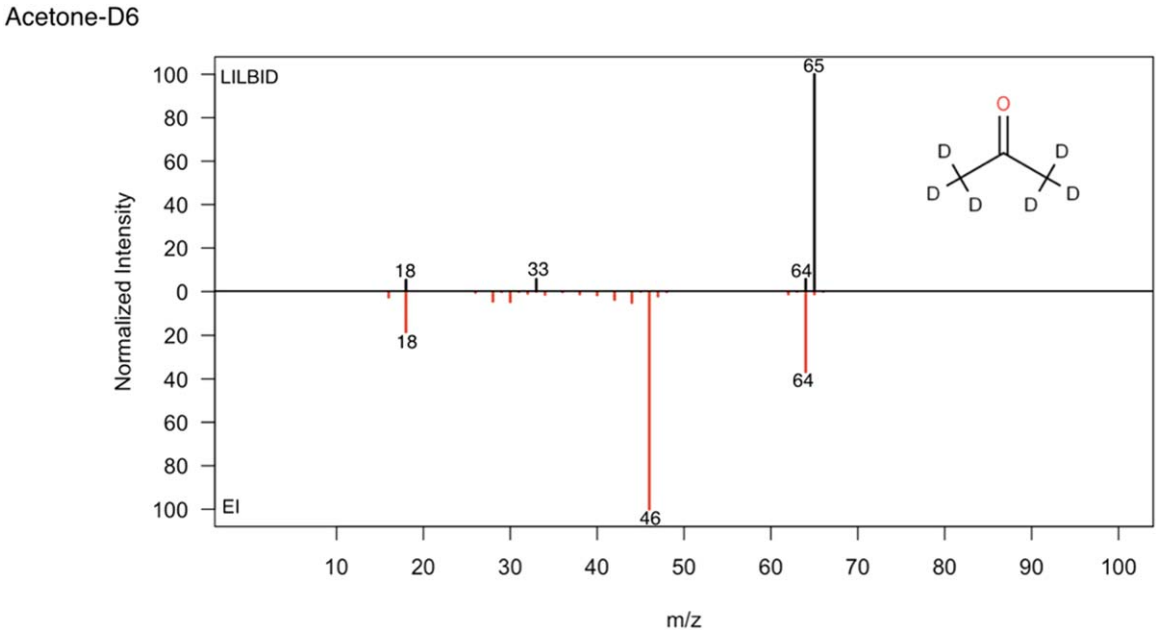

Figure 4. Comparison of LILBID and EI spectra of deuterated acetone-D6. The LILBID (top) produces protonated molecular cations at m/z 65 due to $[C_3D_6O+H]^+$), whereas EI (bottom) produces molecular cations at the exact mass of the acetone-D6 molecule at m/z 64 from $[C_3D_6O)]^+$. The x-axis represents m/z values, and the y-axis shows normalized relative intensity (arbitrary units). For the full spectrum, see Appendix Figure A1(b).

hydronium ion with a neutral organic species (such as $[H_3O]^+(C_3H_5)$). The peak at 50 u might also represent clustering of a neutral species with hydronium, forming $[H_3O]^+(CH_3O)$, as it is not present in the EI spectrum, but the exact nature of this peak is unknown. These kinds of water clusters do not fall into the category of known water clusters (Khawaja et al. 2019; Klenner et al. 2019) mentioned in Section 2.3 that were removed prior to spectral analysis.

The EI spectrum shows a peak at m/z 58 that corresponds to molecular cations $[C_3H_6O]^+$, produced after the removal of an electron from the neutral molecule. In contrast, LILBID generally produces protonated molecular cations of analyte molecules. However, at m/z 59, a Na water cluster $[Na]^+(H_2O)_2$ coincides with the protonated molecular cationic peak of acetone (Appendix Figure A1(a)), as well as that of propanal, and hence is removed from the LILBID spectrum (Figures 3(a) and (b)) as mentioned in Section 2.3. Previously, Klenner et al. (2019) and Khawaja et al. (2019) showed that peak amplitudes of water clusters (H_3O^+, Na^+, and K^+ water) follow a characteristic pattern in LILBID spectra. These water cluster features can overlap with organic cations at the same m/z and cannot be distinguished as separate mass lines due to the insufficient mass resolution of LILBID. In this work, in addition to other water clusters, Na water cluster peaks also follow a certain pattern in acetone and propanal LILBID spectra (Appendix Figures A1(a) and (c)). In the case of acetone, after the first Na water cluster at m/z 41, a sharp increase in the peak amplitude at m/z 59 followed by corresponding Na water clusters is observed. Similarly, in the propanal LILBID spectrum, a subsequent peak at m/z 59 after the peak at m/z 41 should follow the systematic decrease in its amplitude, but instead, an unusual increase is observed. Similar to previous studies (Khawaja et al. 2019; Klenner et al. 2020a, 2020b), we believe that acetone and propanal produce protonated molecular cations in their LILBID spectra at m/z 59.

The LILBID spectra of deuterated acetone-D6 (Figure 4) are produced, which exhibit the feature corresponding to the protonated molecular ions without any interference of known water clusters (Appendix Figure A1(b)) at the same integer mass. This will also show how peaks of Na^+ water clusters follow a systematic pattern in LILBID spectra, and any anomaly in this pattern can be used to identify the contribution of more than one type of cation in the peak amplitude at a certain m/z. The molecular weight of acetone-D6 (from ABCR with 99.9% purity) is 64 u, and a peak at m/z 65 represents protonated molecules ($[M+H]^+$; $[C_3D_6O+H]^+$ in the LILBID spectrum). However, EI produces a molecular peak at the exact mass (64 u) of the molecule. The LILBID also produces a minor peak at m/z 64 due to $[M]^+$. Additionally, peaks at m/z 18 and 33 represent $[CD_3]^+$ and the protonated fragment cation $[CD_2O+H]^+$, respectively. The LILBID spectrum of deuterated acetone proves that, in general, organic compounds measured with LILBID produce protonated molecular cations, as observed not only in this work but also in previous studies (Postberg et al. 2018; Khawaja et al. 2019; Klenner et al. 2020a, 2020b).

In addition, we find no difference in the fragmentation behavior of deuterated as well as normal acetone with EI. In both cases, EI produces the same respective fragment cations, differing only by the mass of the additional deuterium atoms. For example, from normal (protium-containing) acetone, EI produces major cations with masses of 15, 43, and 58 u from $[CH_3]^+$, $[C_2H_3O]^+$, and $[M]^+$, respectively. In the same way, from deuterated acetone, EI forms cations containing deuterium at 18, 46, and 64 from $[CD_3]^+$, $[C_2D_3O]^+$, and $[M]^+$, respectively. However, with LILBID, we find a significant difference between the fragments produced from deuterated and proteated acetone. One major difference is the production of deuterated methenium cations $[CD_3]^+$ at m/z 18 from deuterated acetone through LILBID, with no corresponding production of methenium cations seen in LILBID spectra of proteated acetone or even other nondeuterated carbonyl compounds (Khawaja et al. 2019). Another difference is the absence of $[C_2D_3O]^+$ in LILBID deuterated acetone spectra, which would correspond to the base peak at m/z 43 (i.e., $[C_2H_3O]^+$) in a normal acetone spectrum.

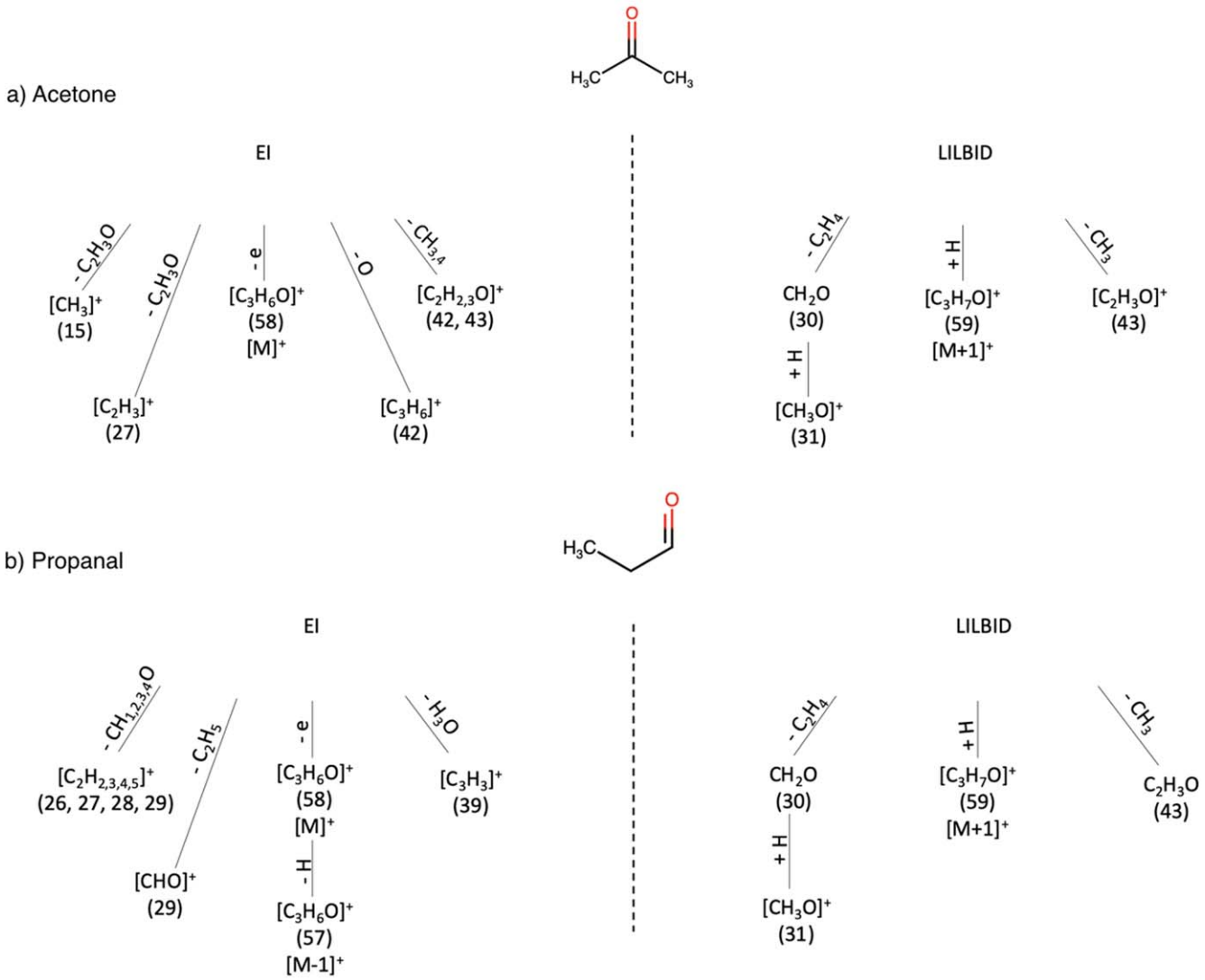

Figure 5. Composition and formation pathways of molecular and fragment cations of (a) acetone and (b) propanal-isomeric carbonyl compounds as produced by EI and LILBID. Organic fragment clusters with water are not shown.

In Figure 3(b), it can be seen that the highest intensity peak in the LILBID propanal mass spectrum is $[C_2H_3O]^+$ at m/z 43, which is not present in the EI propanal spectrum. A contribution to the amplitude of the peak at 43 u could also come from the $[C_3H_7]^+$ carbocation; however, the strong double bond with oxygen in the structure of propanal makes the formation of these fragment cations less likely (Khawaja et al. 2019). The LILBID spectrum of propanal also exhibits a peak at m/z 31 due to $[CH_3O]^+$, whereas this fragment is not visible in the EI spectrum. This ion could form after the cleavage of an alpha bond to produce a CH_2O fragment, which simultaneously gets another hydrogen possibly due to the water matrix to form $[CH_2O{+}H]^+$, where the charge remains on oxygen. In case of EI, due to the lack of a water matrix, the formation of $[CH_3O]^+$ is probably not possible.

The EI spectrum of propanal shows a cluster of peaks in the range 26–29 u corresponding to $[C_2H_2]^+$, $[C_2H_3]^+$, $[C_2H_4]^+$/$[CO]^+$, and $[C_2H_5]^+$/$[CHO]^+$, which is absent in LILBID. In addition, the EI spectrum has a peak at m/z 58 that represents the molecular cationic peak $[M]^+$ of $[C_3H_6O]^+$ and is the base peak in this case. As with the LILBID acetone spectrum, a peak at m/z 59 is present in the LILBID propanal spectrum (Appendix Figure A1(c)) but excluded from the comparison due to the interference with a Na water cluster at this mass line (Figure 3(b)). However, in contrast to the LILBID acetone spectrum, propanal does not exhibit a peak at 60 u, which might be due to the structure of propanal preventing the production of deprotonated cations ($[C_2H_3O\text{-}H]^+$ and subsequently forming its cluster with neutral H_2O. Furthermore, LILBID propanal shows peaks at m/z 81 and 157, which are not present in its corresponding EI spectrum. These peaks might represent the molecular cluster of propanal with Na as $[M{+}Na]^+$ and also the cluster of its dimer species with Na as $[2M{+}H_2O{+}Na]^+$, respectively, but the exact composition of these cations is unknown. Overall, LILBID acetone and propanal spectra exhibit similar characteristic fragments at m/z 31 and 43, whereas the EI spectrum of propanal shows more cation fragments than acetone.

3.2. Carbon-4 Compounds

In this section, we compare the LILBID mass spectra of 2-butanone and butanal, isomeric carbonyl compounds each

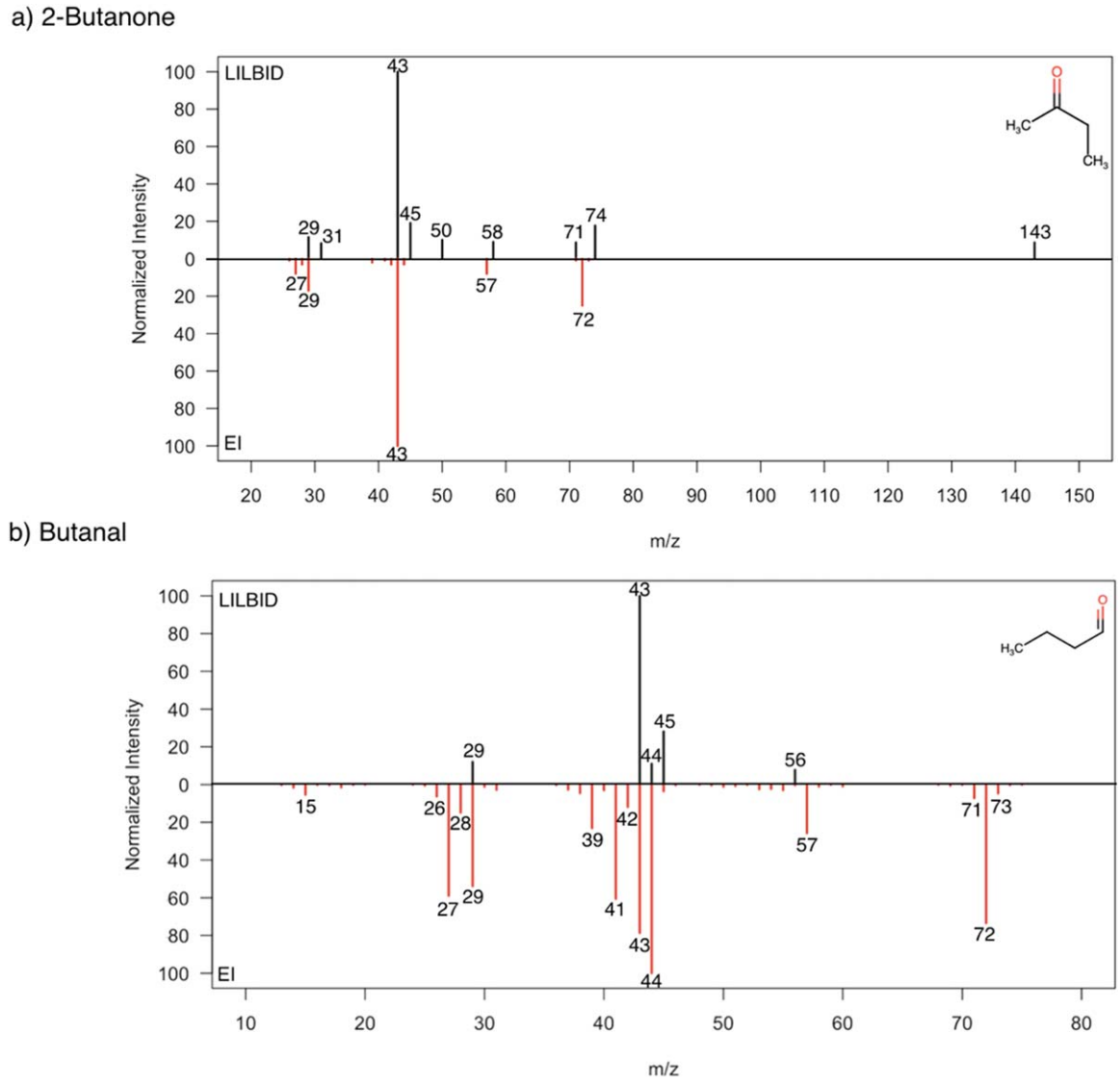

Figure 6. Mirror plots of carbon-4 isomeric carbonyls produced by LILBID (top) and EI (bottom). Panel (a) presents 2-butanone, and panel (b) shows butanal spectra. The *x*-axis represents m/z values, and the *y*-axis represents normalized relative intensities (arbitrary units). For the full spectrum, see Appendix Figure A2.

with one oxygen, four carbon, and eight hydrogen atoms, with their respective EI spectra (Figures 6 and 7).

Figure 6(a) shows a mirror plot of the LILBID and EI spectra of 2-butanone, with peak intensities normalized to the common base peak at m/z 43. Both spectra generally exhibit similar fragment cations, with some exceptions. The peaks at m/z 29 and 43 that correspond to $[C_2H_5]^+/[CHO]^+$ and $[C_3H_7]^+/[C_2H_3O]^+$, respectively, have similar relative intensities. Mass lines at m/z 31 and 45, which correspond to the protonated fragment cations $[CH_3O]^+$ and $[C_2H_5O]^+$, appear only in the LILBID spectrum. A peak at m/z 72 in the EI spectrum represents M^+, the molecular peak $[C_4H_8O]^+$, whereas the LILBID spectrum shows two adjacent peaks at m/z 71 and 74 that are likely to be due to $[M\text{-}H]^+$ and $[M+2H]^+$, respectively. However, these peaks could also be due to clustering of neutral hydrocarbons with hydronium $[H_3O]^+(C_4H_4)$ and $[H_3O]^+(C_4H_7)$. The full LILBID spectrum of 2-butanone (Appendix Figure A2(a)) has a peak at m/z 73 that represents the protonated molecule $[M+H]^+$, but this peak is excluded from further consideration (Figure 6(a)) due to the isobaric interference of a water cluster $[H_3O]^+(H_2O)_3$. The peak at m/z 58 in the LILBID spectrum represents $[M+H\text{-}CH_3]^+$, whereas a nearby 57 u peak in the EI spectrum represents $[M\text{-}CH_3]^+$. However, the peak 58 u in the LILBID spectrum could also potentially represent clusters of neutral organic species with hydronium $[H_3O]^+(C_3H_3)$. The 2-butanone LILBID spectrum also produces the 50 u peak, potentially similar to the hydronium-clustered fragment ion produced by acetone $[H_3O]^+(CH_3O)$.

In the case of butanal, peaks in the LILBID spectrum are normalized to the base peak at m/z 43, whereas peaks in the EI spectrum are normalized to the amplitude of the peak at m/z 44 u (Figure 6(b)). The EI spectrum of butanal shows a greater number of peaks at higher relative intensities in comparison to the LILBID spectrum. In the lower mass range between 26 and 33 u in the LILBID spectrum, butanal produces a peak at m/z 29 due to either $[C_2H_5]^+$ or $[CHO]^+$. The peaks at m/z 27 and 29 in the EI spectrum have significantly higher relative intensities than in the LILBID spectrum. In the intermediate mass range from 39 to 45 u, the LILBID spectrum possesses peaks at m/z 43, 44, and 45, with 43 u $[C_2H_3O]^+$ and 45 u $[C_2H_5O]^+$ being the most prominent. The presence of a minor peak at m/z 26 in EI but absent in LILBID might indicate the

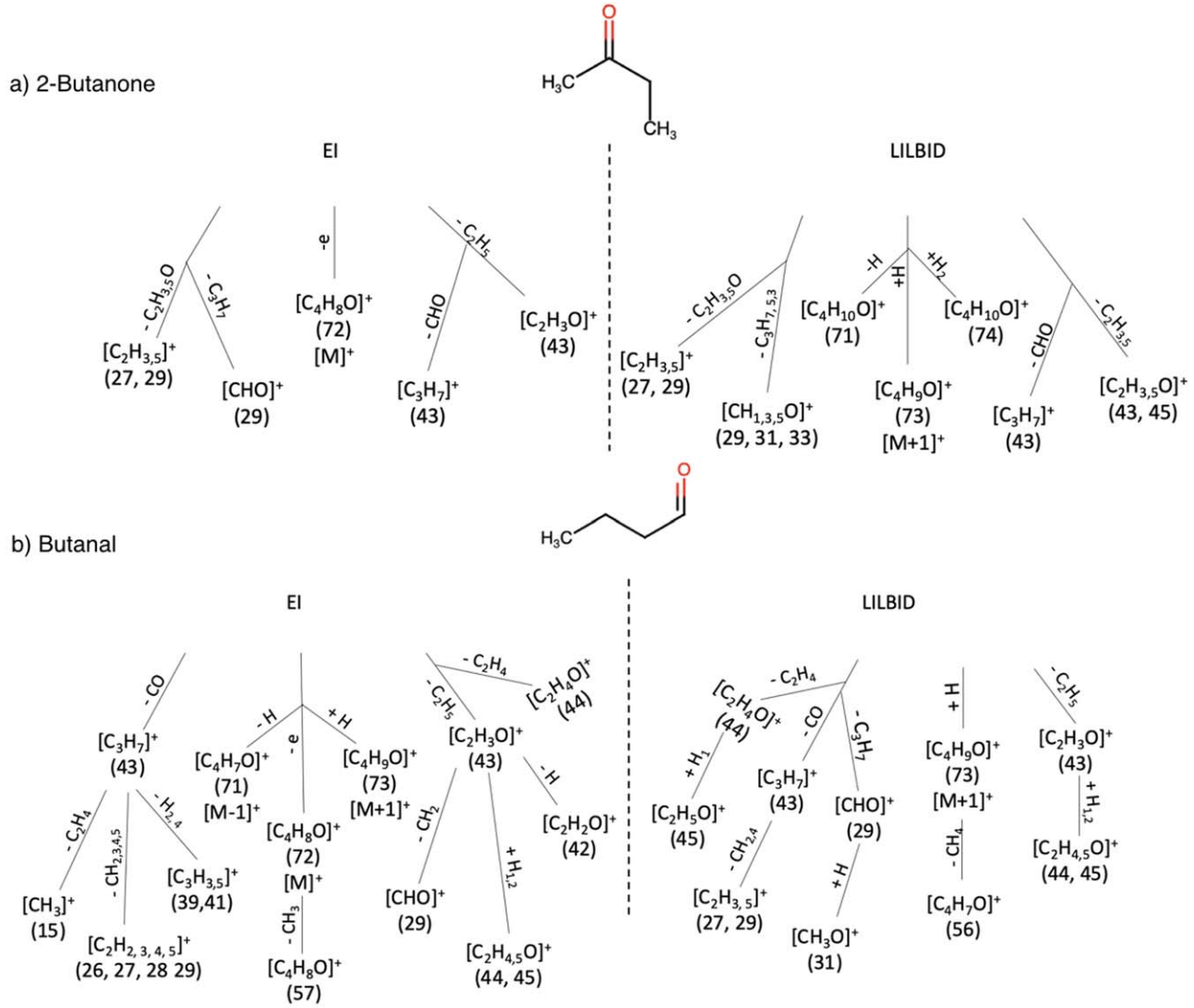

Figure 7. Composition and formation pathways of molecular and fragment cations of a sample of aldehydes and ketones with a carbon number of four. Comparisons of EI and LILBID fragmentation and ionization of (a) 2-butanone and (b) butanal are given.

production of neutral $[C_2H_2]$ with LILBID. In this case, the peak 45 u could be formed due to clustering of neutral organic species with hydronium $[H_3O]^+(C_2H_2)$. In contrast, in this mass range, the EI spectrum has multiple mass lines, at m/z 39, 41, 42, 43, and 44, with the 43 u peak amplitude similar to that in the LILBID spectrum. The 39 and 41 u peaks are only present in the EI spectrum, as in the LILBID spectrum, these peaks could also be formed from $[K]^+$ and $[Na]^+(H_2O)$ (Figures A2(a) and (b)) and therefore were removed from this analysis. However, the contribution from hydrocarbons at these mass lines cannot be excluded. Unlike the LILBID spectrum, in which the base peak is at m/z 43, in the EI spectrum, the base peak is at m/z 44 from $[C_2H_3O]^+$ and $[C_2H_4O]^+$, respectively.

The peaks at m/z 39 and 41 are hydrocarbon fragments ($[C_3H_3]^+$, $[C_3H_5]^+$) in the EI butanal spectrum but not observed in the EI 2-butanone spectrum (Figure 6). Like 2-butanone, butanal also produces a peak at m/z 45 via LILBID, which is not observed in the EI spectrum. In the mass range between 71 and 73 u, the EI butanal spectrum has a much stronger molecular peak $[M]^+$ at m/z 72 when compared to 2-butanone. The two minor adjacent peaks at m/z 71 and 73 in butanal are most likely due to protonated $[M+H]^+$ and deprotonated $[M\text{-}H]^+$ molecular cations. As with 2-butanone, in the full LILBID spectrum of butanal (Appendix Figure A2(b)), there is a peak at m/z 73 that could potentially correspond to the protonated molecular cation $[M+1]^+$, but due to the interference with the water cluster $[H_3O]^+(H_2O)_3$, it is excluded in the comparison with the EI spectrum. In contrast to 2-butanone, peaks corresponding to deprotonated and potential isotopic molecular cations are not present in the LILBID spectrum of butanal (Appendix Figure A5). The peak at m/z 56 in the LILBID spectrum represents the $[M+H\text{-}OH]^+$ ion, whereas the peak at m/z 57 in the EI spectrum represents that of $[M\text{-}CH_3]^+$.

In general, 2-butanone and butanal in LILBID produce similar fragments, whereas in EI, the butanal tends to produce more fragments, which differ significantly from those produced by LILBID. The EI has a tendency to produce hydrocarbon fragment cations (39 and 41 u) from butanal that are not produced from 2-butanone. This trend is in agreement with the molecular structure of butanal, which favors the generation of carbocations carrying three carbons by cleavage of the C–C alpha bond within the molecule. In contrast to the EI spectra, in LILBID spectra of both compounds (Appendix Figure A5), a

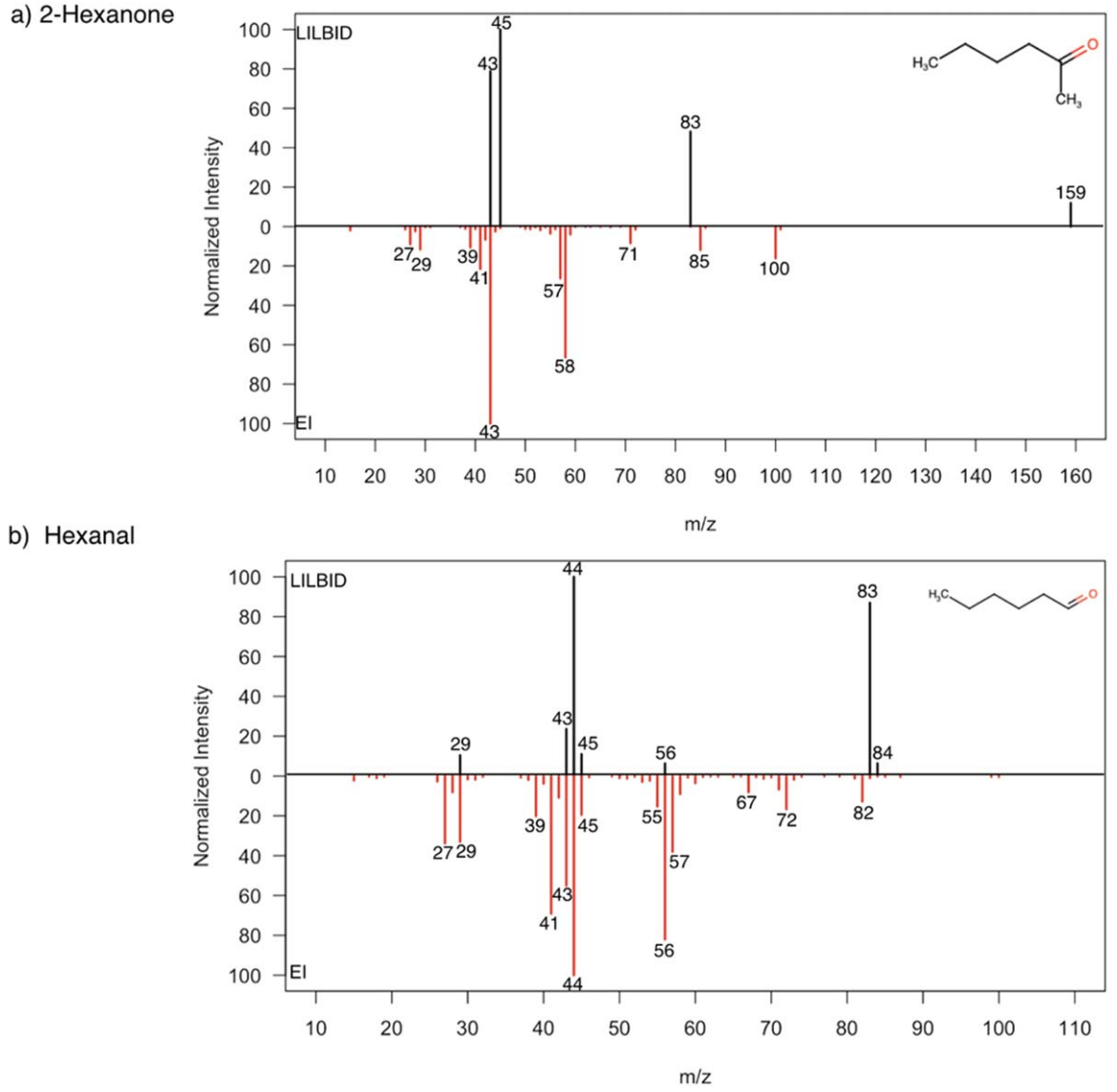

Figure 8. Mirror plots of carbon-6 isomeric carbonyls produced by LILBID (top) and EI (bottom). The comparison between mass spectra of (a) 2-hexanone and (b) hexanal are shown. The *x*-axis represents m/z values, and the *y*-axis represents normalized relative intensities (arbitrary units). For a full spectrum, see Appendix Figure A3.

protonated peak is observed at m/z 45, demonstrating the tendency of molecular fragments to protonate in the water matrix. In EI spectra, $[M]^+$ molecular peaks are observed at 72 u, whereas in the LILBID spectra, protonated peaks $[M+H]^+$ at m/z 73 (Appendix Figure A2(b)) are expected to be observed that interfere with water clusters and hence are excluded from this comparison.

3.3. Carbon-6 Compounds

In this section, the isomeric carbonyl compounds 2-hexanone and hexanal are analyzed. These compounds contain one oxygen, six carbon, and 12 hydrogen atoms (Figures 8 and 9).

The LILBID and EI spectra of 2-hexanone are normalized by the intensities of the peaks with the highest amplitudes in the spectra, at m/z 45 and 43, respectively (Figure 8(a)). The LILBID spectrum has no peaks (greater than the applied threshold of 0.003 for relative intensity) in the range 26–33 u; however, it shows a prominent peak at a higher mass, m/z 83. In the range 39–45 u, the peak at m/z 43 ($[C_2H_3O]^+$/ $[C_3H_7]^+$) is large (80% of the base peak at 45 u). This base peak, from $[C_2H_5O]^+$, is unique to LILBID and its tendency for protonation. Similarly, the prominent peak at m/z 83 is only present in the LILBID spectrum, which represents the loss of OH from the 2-hexanone molecule during the McLafferty rearrangement process. The formation of such ions is not characteristic of the McLafferty mechanism; rather, they are typical of carbonyl compounds that are measured with LILBID, which at least have three carbons in the side chain of their molecules. The protonated molecular peak at m/z 101 $[M+H]^+$ is observed in the full LILBID spectrum (Appendix Figure A3(a)) but potentially interferes with the water cluster $[M\text{-}OH]^+(H_2O)$ and is removed for comparison with the EI spectrum (Section 2.3; Figure 8(a)). Additionally, the LILBID spectrum shows a peak at m/z 159, above the molecular mass of 2-hexanone and perhaps related to clusters such as $[M+Na+2H_2O]^+$, but the exact composition cannot be inferred. The EI spectrum has peaks at m/z 71, 85, and 100

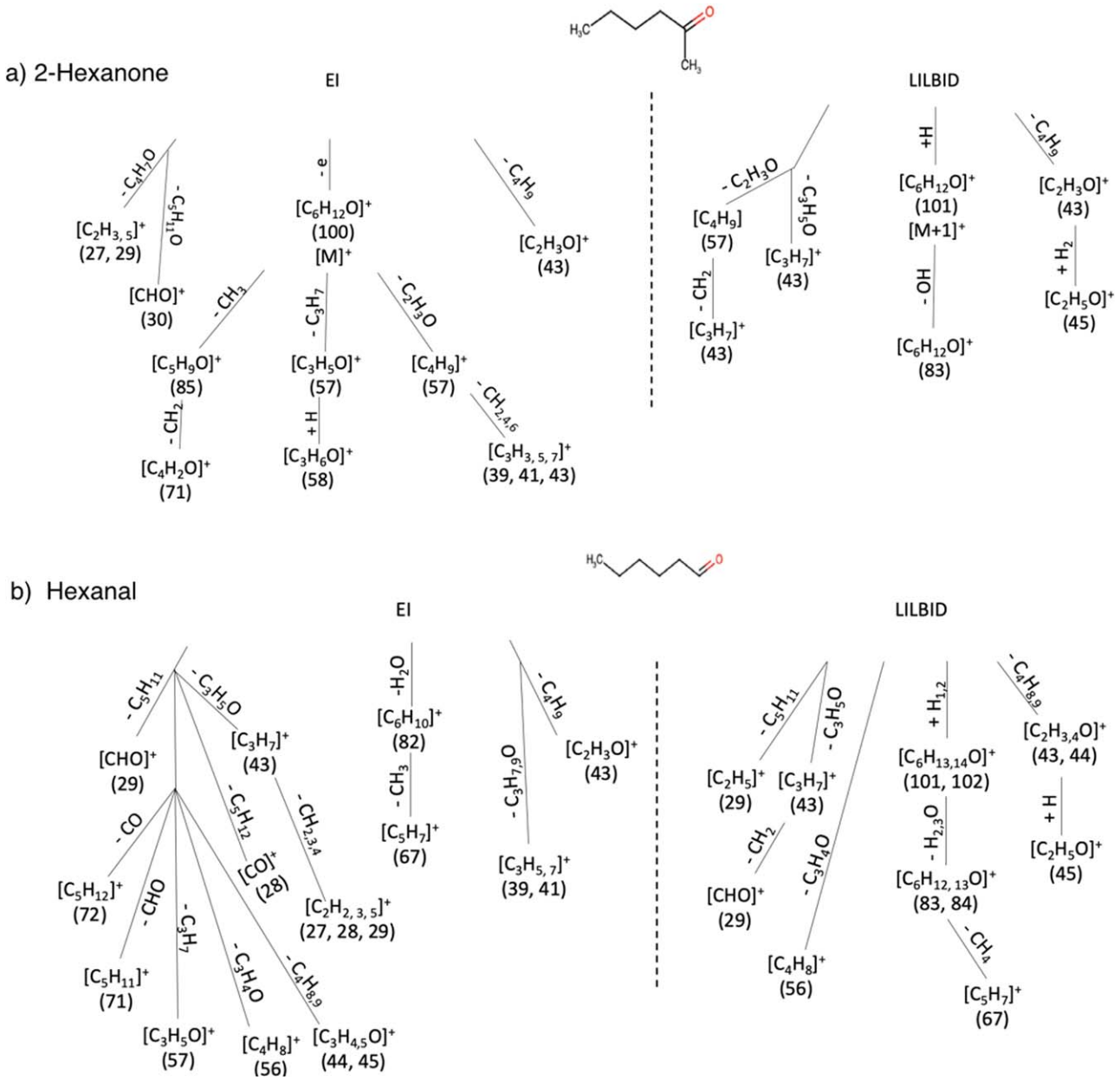

Figure 9. Composition and formation pathways of molecular and fragment cations of (a) 2-hexanone and (b) hexanal- carbonyl compounds with six carbon atoms as produced by EI and LILBID.

that correspond to $[M\text{-}C_2H_5]^+$, $[M\text{-}CH_3]^+$, and $[M]^+$, respectively. The peaks at m/z 27, 29, 39, and 41 are from hydrocarbon fragment cations ($[C_2H_3]^+$, $[C_2H_5]^+$, $[C_3H_3]^+$, and $[C_3H_5]^+$), which are either not present in the LILBID spectrum or, in the case of the 39 and 41 u peaks, removed due to potential interference from $[K]^+$ and $[Na]^+(H_2O)$; Section 2.3). The double peaks at m/z 58 and 57 are another major difference between both spectra, where 58 u could be $[M\text{-}CH_3\text{-}C_2H_3]^+$ or $[M\text{-}C_2H_3O\text{+}H]^+$, and 57 u could be $[M\text{-}CH_3\text{-}C_2H_3\text{-}H]^+$ or $[M\text{-}C_2H_3O]^+$.

With hexanal (Figure 8(b)), the base peak at m/z 44, from $[C_2H_4O]^+$, is used for the normalization of peaks in both the LILBID and EI spectra. The triplet of peaks at m/z 43, 44, and 45 has abundance patterns that match between the two spectra. In LILBID, a prominent peak at m/z 83 is observed, identified as due to $[M\text{-}OH]^+$, and not present in the EI spectrum. As previously discussed for 2-hexanone, these ions are not characteristic of McLafferty rearrangement (McLafferty & Turecek 1993) itself. We find the formation of $[M\text{-}OH]^+$ very typical for LILBID that might be possible during McLafferty rearrangement of the carbonyl molecules, which have at least three carbons in the side chain of the molecule. The molecular cationic peak is not observed in both LILBID and EI hexanal spectra. Furthermore, in LILBID, a small peak at m/z 29, identified as from $[C_2H_5]^+$ and/or $[CH_3O]^+$, is observed. In the EI spectrum, this peak has a higher relative amplitude and appears together with a distinct peak at m/z 27 from $[C_2H_3]^+$. The EI spectrum also exhibits peaks at m/z 39 and 41 that are known to be from $[C_3H_3]^+$ and $[C_3H_5]^+$ and were removed from the LILBID spectrum due to the potential interference from $[K]^+$ and $[Na]^+(H_2O)$ at these masses (Figure A3). A cluster of peaks is observed in the EI spectrum at m/z 55–57, with the highest-amplitude peak at m/z 56 identified as from $[M\text{-}C_2H_4O]^+$, which also appears in the LILBID spectrum. In

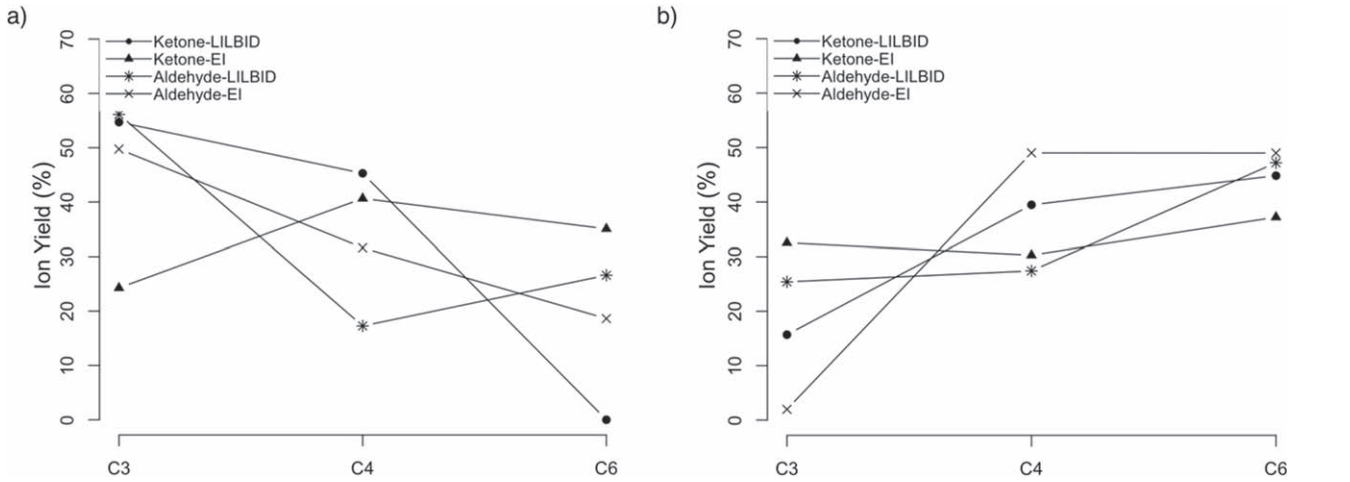

Figure 10. Percentages of cumulative relative intensities (ion yields) of all mass lines corresponding to LILBID- and EI-produced fragment cations within mass ranges (a) 26–33 and (b) 41–45 u for ketones and aldehydes with carbon numbers of three, four, and six. The *x*-axis represents the number of carbon atoms, where C3, C4, and C6 stand for carbon three, four, and six compounds, respectively. The *y*-axis represents the accumulative relative intensities.

LILBID spectra of hexanal, as well as in butanal, a peak at m/z 56 indicates the formation of clustering neutral organic species with hydronium $[H_3O]^+(C_3H)$.

In general, EI hexanal and 2-hexanone spectra show a higher number of cationic fragments in comparison with the corresponding LILBID spectra. Overall, both compounds show similar features in their LILBID spectra (Appendix Figure A6), with the major exception of the base peak, which is at m/z 45 in 2-hexanone and 44 in hexanal. In EI spectra, a significant number of fragments in high abundance are observed in hexanal as compared to 2-hexanone.

3.4. Correlation

To help understand differences in the fragmentation processes of these small molecules, the correlation between the carbon number (three to six) in carbonyl compounds and the production of positive ions within particular mass ranges, (a) 26–33 u and (b) 41–45 u (Figure 10), was investigated.

In the mass range 26–33 u, the EI data of ketones show an increase in the relative abundances of ions (24%–40%), with the greatest increase from three (24%) to four (40%) carbons but then slightly lower for the higher carbon number. However, ketones with LILBID show much a higher abundance (55%) for carbon three as compared to the corresponding EI (25%) but then show a decreasing trend from 55% to 50% as the number of carbons increases from three to four and a sharp decrease to 0% for carbon six. This indicates that LILBID causes more fragmentation of ketones containing three carbons and EI produces more ions for ketones having six carbons, whereas ketones with four carbons show similar relative intensities with both the LILBID and EI in the range of 26–33 u. In the case of aldehydes, both LILBID and EI show a generally negative correlation between ion production and the number of carbons in the molecule. Both ionization methods produce a higher number of ions from carbon three aldehydes as compared to four and six carbon compounds. In the case of EI, aldehydes show a gradually decreasing trend from 50% to 20% with an increasing number of carbons, and, with LILBID, abundances of aldehyde fragments sharply decrease from three to four carbons (55% to 18%) but then increase to 30% for six carbon compounds.

In the mass range 41–45 u, the LILBID spectra of ketones show an increase in relative peak intensity values (∼15%–45%) with increasing carbon number. However, the EI spectra of ketones show no significant change in the relative intensities within this mass range. Production of 41–45 u fragment ions by LILBID therefore exhibits a positive correlation with carbon number, whereas the relative intensities of fragment ions with EI have not influenced the size of the molecule. For aldehydes, EI produces a significant increase in relative intensities from 0% to 50% from carbon three to four and remains unchanged for carbon six. The LILBID production of 41–45 u fragments from aldehydes exhibits almost the completely opposite behavior, with only a slight increase in the relative intensities as the carbon number increases from three to four, followed by a significant increase for carbon six, from approximately 25% to 45%. In general, except for ketones measured with EI, for which the production of fragment ions in this mass range does not seem to strongly correlate with molecule size, we observe a positive correlation between the parent molecule carbon number and the ion production in the mass range 44–45 u.

In the mass range between 26–32 and 41–45 u (Figures A4–A6), LILBID spectra show similar fragment ions for carbon three and four carbonyls. With the increased molecular size, ketones and aldehydes show different fragment ions. Carbon three (acetone and propanal), as well as carbon four compounds (2-butanone and butanal), show mass lines in their LILBID spectra that correspond to similar fragment ions, e.g., 31 and 43 u in the case of carbon three and 29, 43, and 45 u in the case of carbon four compounds. For carbon six compounds, LILBID spectra of 2-hexanone and hexanal show a significant difference in these mass ranges. The 2-hexanone shows fragment ions in the mass range of 26–32 u, whereas hexanal shows fragment ions at m/z 29. Both compounds also show similar fragment ions at m/z 43 and 45, where 2-butanone shows a significant abundance of these ions as compared to butanal. On the other hand, butanal shows fragment cations corresponding to 44 u, which is not observed in 2-butanone.

For both the ketones and aldehydes, the peak ratio $(44+45)/(43)$ u clearly shows (Appendix Figure A7) an increase with the increased size of the parent molecule from carbon three to six. The fragmentation of the parent molecule to produce $(44+45)$ u is even more pronounced in aldehydes as compared to ketones. This ultimately indicates that the molecular structures of large-sized aldehydes and ketones can

Table 2
Organic Fragment Cations in LILBID Spectra of Carbonyls Can Be Inferred from Their Respective EI Spectra

m/z	EI	LILBID	Complementary Differences
29	$[CHO]^+/[C_2H_5]^+$	$[CHO]^+/[C_2H_5]^+$	If EI produces a fragment at m/z 29, LILBID will also form a fragment at m/z 29 and/or 31.
31	⋯	$[CH_3O]^+$	In general, this fragment is specific only to LILBID.
43	$[C_2H_3O]^+/[C_3H_7]^+$	$[C_2H_3O]^+/[C_3H_7]^+$	If EI produces fragments in the range 39–44 u, LILBID will also form a fragment at m/z 43 and/or 44–45.
45	⋯	$[C_2H_5O]^+$	In general, this fragment is specific only to LILBID, except for EI hexanal.
*	$[M]^+$	$[M+1]^+$	In general, EI produces molecular peaks, but LILBID produces protonated molecular peaks.
	⋯	$[M\text{-}OH]^+$	Furthermore, LILBID also produces another fragment after removal of OH from the molecule.

Note. The asterisk refers to the m/z of any molecular cation.

be differentiated from the smaller size based on the peak ratio $44 + 45/43$ u. This might also show that the McLafferty rearrangement mechanism is occurring efficiently in bigger carbonyl molecules, particularly in aldehydes.

Due to the difference between the ion source and the initial environment, LILBID and EI mostly produce different fragments and fragmentation patterns of organic compounds. However, despite the difference in fragmentation, we demonstrate that both techniques could still complement each other for the identification of organic species (Table 2), which has implications for spaceborne impact ionization and EI mass spectrometers, e.g., SUDA and MASPEX on board NASA's Europa Clipper space mission. While there are differences in fragmentation behavior in aldehydes and ketones for both techniques, EI and LILBID best complement the identification of C3 and C4 ketones and C6 aldehydes embedded in ice grains.

For example, the EI method produces a molecular ionic peak $[M]^+$, whereas LILBID produces the corresponding protonated peak $[M+1]^+$. Similarly, from EI spectral features in the mass range between 26–33 and 39–45 u, the presence of protonated fragments at m/z 31 and 45 in LILBID spectra can be inferred for different carbonyl compounds. Typically, EI produces fragment ions between m/z 26–33 and 39–45 from hydrocarbons, but in some cases (e.g., hexanal), the oxygen-carrying fragment at 45 u can also be observed. However, in LILBID, most of the protonated fragments in the mass ranges 29–31 and 43–45 u are generated by these oxygen-carrying ions. For example, fragment ions at 29 and 43 u are produced by EI, as well as LILBID; however, 31 and 45 u are protonated ions that are generally produced by LILBID.

The commonly observed acylium ion at m/z 43 in EI ketone spectra is due to the cleavage of the alpha bond (next to the carbonyl bond). In this way, the most stable acylium ions form the base peak in ketone mass spectra. In the spectra of larger linear ketones, peaks at 57 and 71 u are also observed with a mass difference of $\Delta m \approx 14$ from 43 u to form spectral features in a sequence such as $(43 + 14 = 57)$ and $(57 + 14 = 71)$ u, e.g., in 2-butanone and 2-hexanone spectra, respectively. In addition, a fragment ion, $[M\text{-}OH]^+$, also occurs as a result of the elimination of OH from the molecule during McLafferty rearrangement (McLafferty & Turecek 1993). The elimination of OH and the protonation of ions is typical for LILBID spectra. This process is probably a consequence of the water matrix, which is not present in the case of EI. The formation of $[M\text{-}OH]^+$ occurs in the LILBID-tested aldehydes and ketones with a carbon number $\geqslant 4$ where the side chain of the molecule contains at least three carbon atoms, in which case, McLafferty rearrangement is also possible. In these carbonyls, $[M\text{-}OH]^+$ could be formed when the oxygen on the primary carbon accepts a hydrogen atom from the gamma-carbon of the parent molecule to form an OH functional group. This then cleaves from the carbon backbone, resulting in the $[M\text{-}OH]^+$ fragment cation. However, we cannot rule out the formation of an ion at the same mass after the loss of water from the protonated molecular ion. In 2-hexanone and hexanal, the $[M\text{-}OH]^+$ peak is at m/z 83 (Figure 8), whereas in 2-butanone and butanal, this fragment forms at m/z 55 (Khawaja et al. 2019). However, in this latter case, the peak at 55 u coincides with the water cluster $[H_3O]^+(H_2O)_2$ (Figure A2) and is thus removed from the mirror plot (Figure 6).

In another process, carbonyl compounds could be protonated in the water matrix first and then eliminate water from the protonated molecule to form the fragment cation $[M+H\text{-}H_2O]^+$ of the same mass as $[M\text{-}OH]^+$ formed as a by-product during the McLafferty mechanism typical for LILBID. Therefore, we cannot rule out any of the processes to form either ions $[M\text{-}OH]^+$ or $[M+H\text{-}H_2O]^+$ at the same mass in carbonyl compounds, which have at least three carbon atoms in the side chain of the molecule. In EI, aldehydes that have at least three carbon atoms at the side chain of the molecule produce ions at m/z 44 characteristic of the McLafferty rearrangement. The absence of the production of $[M\text{-}OH]^+$ in EI spectra but its presence in the LILBID spectra of those carbonyls where McLafferty is also possible indicates a dependence of this fragment or its production on the water matrix.

In the case of carbon three carbonyls (acetone and propanal), elimination of OH from the parent molecule is not possible due to the lack of carbon atoms in the side chain to form $[M\text{-}OH]^+$ at m/z 41. However, the loss of water molecules from the protonated molecular ion might be possible to form cations at m/z 41. However, the peak 41 u could also be due to $[Na]^+(H_2O)$ and hence is removed from the analysis (Appendix Figures A1(a) and (c) and 3).

4. Conclusions

A comparative study of the mass spectra of three groups of isomeric aldehydes and ketones using spectra from the NIST EI online reference library, as well as those produced via LILBID from their aqueous solutions, has been undertaken. We demonstrate that differences in the mass spectral features produced by different spaceborne mass spectrometers could complement each other for elucidating the structural properties of unknown organic species (Table 2).

A greater number of different fragment cations were observed at higher abundances in EI aldehyde spectra than in their respective LILBID spectra. The EI aldehyde spectra also exhibit a higher number of fragment cations than EI ketone spectra. The

LILBID produces similar fragments from ketones and their respective isomeric aldehydes (Figures A4, A5, and 1). In general, ketones produce similar abundances of major fragment cations in their EI and LILBID spectra. In addition, 2-hexanone produces more fragment cations via EI at higher abundances than in the corresponding LILBID spectrum. The EI and LILBID spectra of both ketones and aldehydes produce fragment cations at the highest abundances between m/z 43 and 45, forming the spectral base peaks, with the notable exception of EI propanal, where the base peak is due to the molecular cation $[M]^+$ at m/z 58. We could not find any clear trend of clustering of neutral organic species with $[H_3O]^+$ or $[Na]^+$; however, some not definitively identified spectral features might correspond to neutral hydronium clustering, such as $[H_3O]^+(CH_3O)$, $[H_3O]^+(C_3H_5)$, $[H_3O]^+(C_3H_3)$, $[H_3O]^+(C_4H_4)$, $[H_3O]^+(C_4H_7)$, $[H_3O]^+(C_3H)$, and $[H_3O]^+(C_2H_2)$. The detection of deuterated methenium cations $[CD_3]^+$ at 18 u, in comparison with the relative paucity of proteated methenium ions $[CH_3]^+$ at 15 u, along with the identification of protonated deuterated formyl species $[CD_2O+H]^+$ in LILBID spectra, indicates that impact ionization (as simulated by the LILBID technique) will provide a valuable tool for identifying fragment cations (likely characteristic) from deuterated organic compounds. We also observed that instead of producing formyl cationic species, the EI spectrum shows deuterated acylium cationic species $[C_2D_3O]^+$ in addition to deuterated methenium cations $[CD_3]^+$.

For EI, a positive correlation is observed between the relative intensities of mass lines in the mass range 26–33 u and the carbon number (from three to four) of the parent ketone, with a slight decrease in intensities for carbon six. However, in LILBID, this is reversed, with a negative correlation found for the intensities of mass lines in the 26–33 u region in ketones with increasing carbon number. However, a positive correlation is observed in the LILBID spectra of ketones between the relative intensities of mass lines in the mass range 41–45 u and the carbon number of the parent molecule, whereas in EI, ketones show no change in the relative intensities of mass lines in this mass range. For EI, the spectra of aldehydes show a negative correlation between the carbon number and the relative intensities in the mass range 26–33 u, a phenomenon also observed in LILBID from carbon numbers three to four but which then reverses from carbon numbers four to six. For aldehydes, in EI spectra in the mass range 41–45 u, we observe a positive correlation between the intensities of mass lines and the carbon number from three to four, which then flattens between butanal and hexanal. In LILBID, a positive correlation is observed between relative intensities and the carbon number across the entire range. In general, for ketones in LILBID and aldehydes in EI, a significant correlation is observed between carbon numbers in the parent molecule and relative intensities in the mass ranges 26–33 and 41–45 u. The ratio of relative intensities, $44+45/43$, indicates that larger carbonyl compounds produce more fragments at masses 44 and 45 u than smaller carbonyl compounds, which tend to produce more fragments at mass 43 u.

From the EI spectra of the considered aldehydes and ketones, some of the characteristic fragments of these compounds that will be found in their LILBID spectra can be inferred. These compounds produce molecular cations $[M]^+$ in their EI spectra, whereas their LILBID spectra generally possess protonated molecular cations $[M+H]^+$. We could also infer the presence of $[M\text{-}OH]^+$ fragment cations in the LILBID spectra of carbonyl compounds having four or more carbon atoms with at least three carbon atoms in the side chain after McLafferty rearrangement and further scission, which is typical of LILBID only. In general, EI spectra exhibit peaks attributable to the hydrocarbon fragments $[C_2H_{2,3,4,5}]^+$ and $[C_3H_{3,5,7}]^+$ in the mass ranges 26–29 and 39–45 u. However, LILBID produces mainly oxygen-carrying fragments at m/z 29 and 43 ($[CHO]^+$ and $[C_2H_3O]^+$, respectively) and also tends to produce the corresponding protonated ions at m/z 31 and 45 ($[CH_3O]^+$ and $[C_2H_5O]^+$).

We observed similarities and differences in the composition of the characteristic ions produced by EI and LILBID. Despite the differences, we demonstrate that fragments produced by LILBID and EI complement each other for the identification of compounds with unknown compositions. We also show that the online EI NIST mass spectral library can be a useful source for the analysis of mass spectra obtained by LILBID, a technique that is used to simulate the impact ionization mass spectra of ice grains recorded in space, and vice versa. This work provides initial guidelines that can be employed for the interpretation of impact and EI mass spectral data, specifically the data that will be obtained from, e.g., NASA's future Europa Clipper space missions (Howell & Pappalardo 2020; Cable et al. 2021) toward Jupiter's moon Europa.

The authors thank Wilhelm Zuschneid for his valuable feedback.

This work was supported by European Research Council (ERC) Consolidator Grant 724908-Habitat OASIS.

Appendix
Supplementary Data

A.1. Coadded LILBID Spectra

The LILBID spectra of all three DTs (Section 2.3) of each compound (measured at 0.05 molar concentration) are coadded without removing any water cluster features (Figures A1–A3). In these spectra, peaks at the same integer mass with an amplitude $\geqslant$0.003 relative intensity were coadded. The absence of certain peaks in the mirror plot (Figures 3–6) and presence in the coadded plot is because that particular peak was either absent (or below the applied amplitude threshold) for a certain DT but appeared at another DT.

In these figures, blue mass lines represent water clusters $(H_3O^+).(H_2O)_{n=0,1,2...}$, red represents Na water clusters $(Na^+).(H_2O)_{n=0,1,2...}$, and green represents K water clusters $(K^+).(H_2O)_{n=0,1,2...}$. Black lines represent organic cations and their water clusters. The x-axis shows m/z values, and the y-axis represents intensity in log scale.

A.2. LILBID Ketone versus Aldehyde Mirror Plots

The mirror plots of LILBID spectra of ketones and aldehydes are represented in Figures A4–A6. In these spectra, only organic features at the same integer mass with an amplitude $\geqslant$0.003 relative intensity obtained from three different DTs are compared (Section 2.3). All compounds in this work are measured at 0.05 molar concentration with three DTs that are combined here according to the selection criteria described in the main text (Section 2.3). The x-axis shows m/z values, and the y-axis represents normalized relative intensity values.

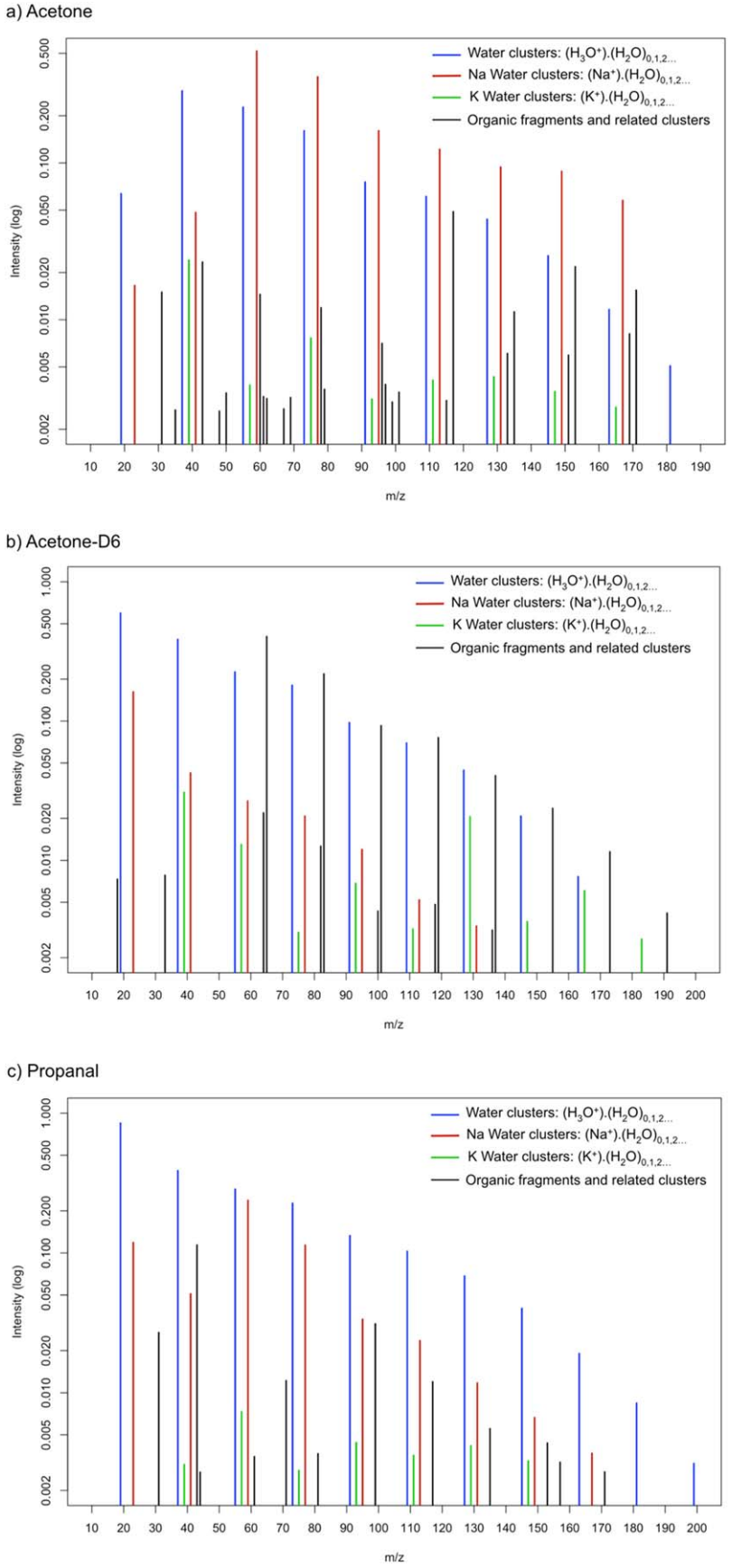

Figure A1. LILBID spectra of (a) acetone, (b) acetone-D6, and (c) propanal. Acetone-D6 is measured to demonstrate that LILBID produces a protonated molecular peak of the analyte compound. It is not possible to differentiate this peak in other compounds in this work due to the interference of water cluster features at the same mass.

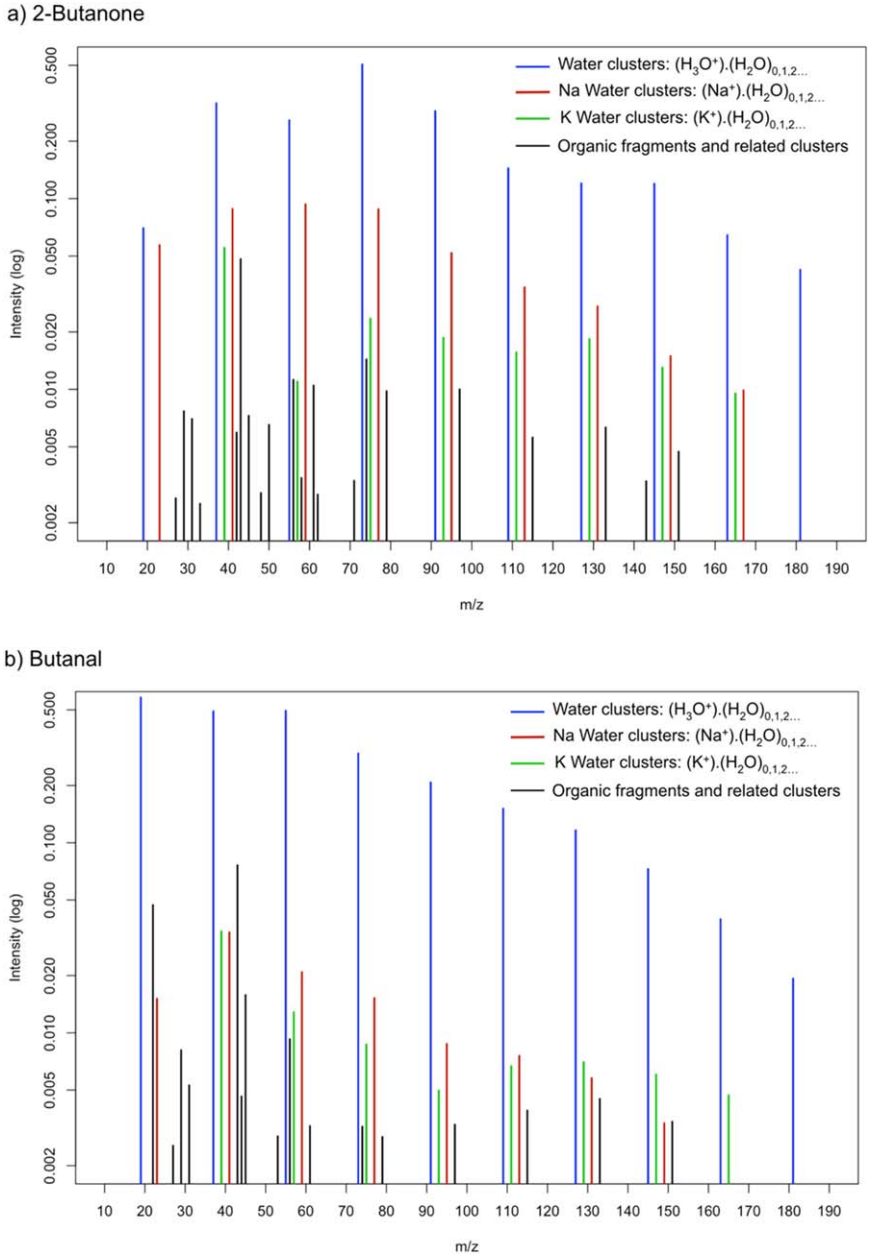

Figure A2. LILBID spectra of (a) 2-butanone and (b) butanal.

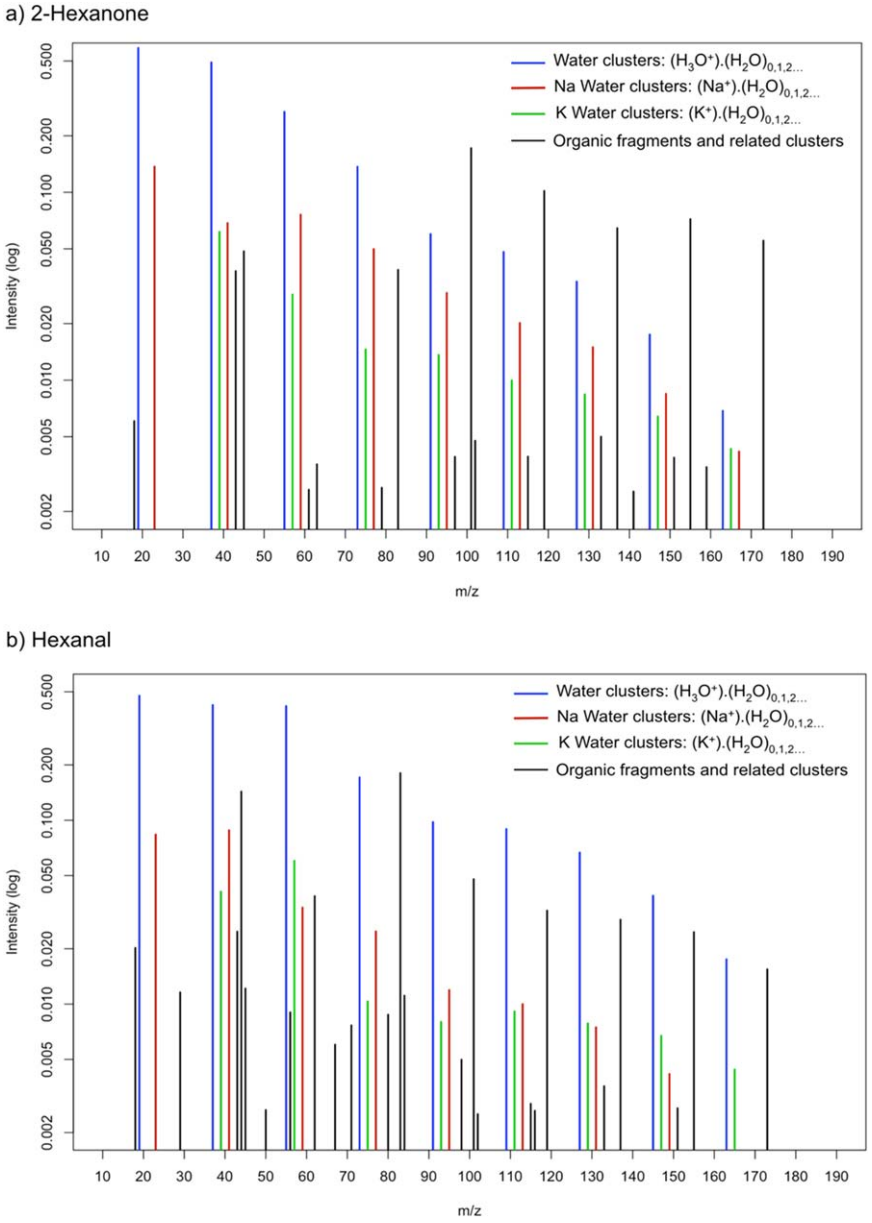

Figure A3. LILBID spectra of (a) 2-hexanone and (b) hexanal.

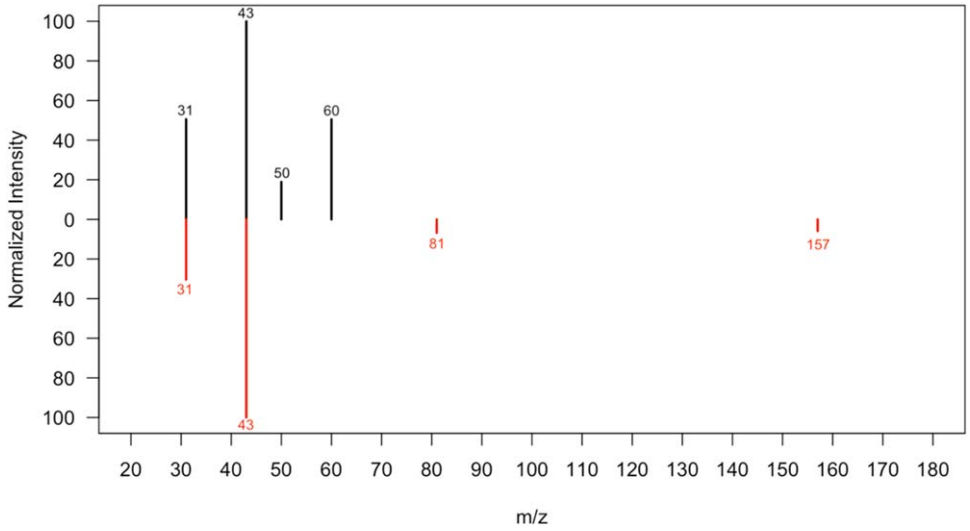

Figure A4. Normalized relative intensity LILBID mirror plot for acetone (black) and propanal (red).

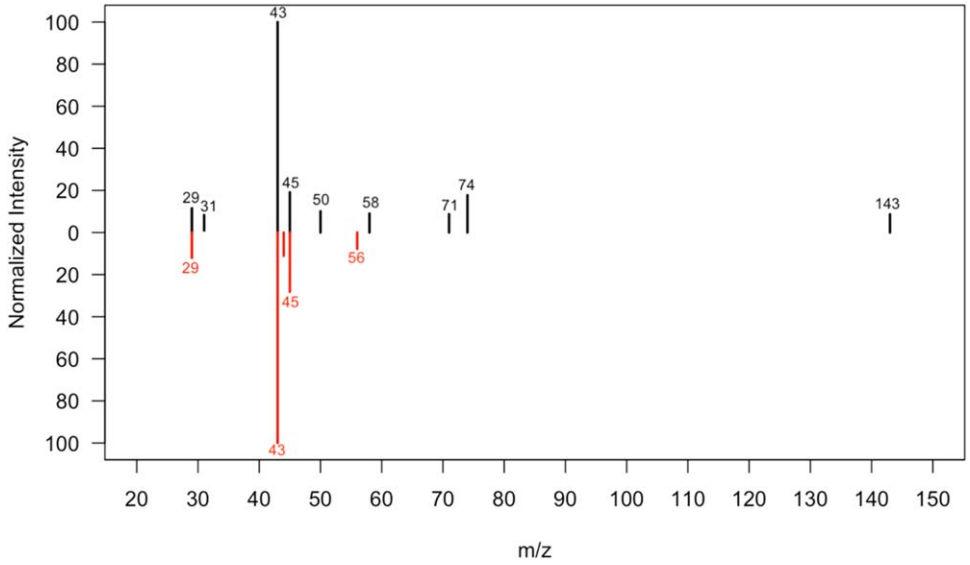

Figure A5. Normalized relative intensity LILBID mirror plot for 2-butanone (black) and butanal (red).

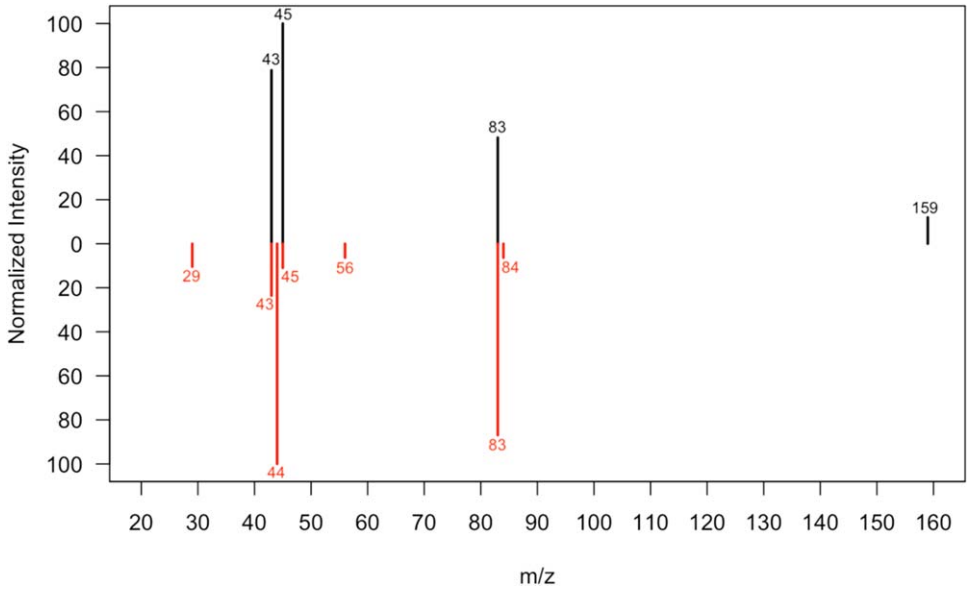

Figure A6. Normalized relative intensity LILBID mirror plot for 2-hexanone (black) and hexanal (red).

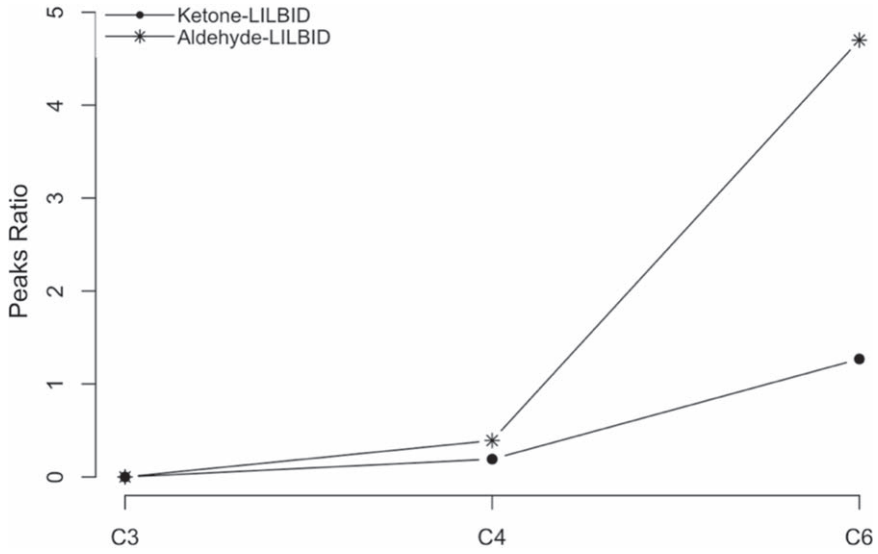

Figure A7. Peak ratio of relative intensities of 44, 45, and 43 u, such as $44 + 45/43$, corresponding to LILBID-produced fragment cations for ketones and aldehydes with carbon numbers of three, four, and six. The *x*-axis represents the number of carbon atoms, where C3, C4, and C6 stand for carbon three, four, and six compounds, respectively. The *y*-axis represents the peak ratio.

Table A1
The Mass Lines and Normalized Intensities of Ketones, i.e., Acetone, 2-butanone, and 2-hexanone, Are Presented Here at Combined DTs without Water Clusters

Comparison of Ketone Mass Spectra (Normalized Intensities)						
Carbonyl Type	Ketones					
Compound	Acetone		2-Butanone		2-Hexanone	
Chemical formula	CH_3CH_2CHO		$CH_3(CH_2)_2CHO$		$CH_3(CH_2)_4CHO$	
Carbons	3		4		6	
Mol. weight	58		72		100	
Library	LILBID	EI	LILBID	EI	LILBID	EI
m/z						
13	0	0.89	0	0	0	0
14	0	4.55	0	0	0	0.2
15	0	12.01	0	4	0	1.9
16	0	0.85	0	0	0	0
25	0	1.29	0	0	0	0
26	0	4.96	0	1	0	1.4
27	0	7.07	0	8	0	9.01
28	0	1.21	0	3	0	2.4
29	0	3.62	11.54	17	0	11.61
30	0	0	0	0	0	0.3
31	50.54	0.45	8.29	0	0	0.3
33	0	0	0	0	0	0
36	0	0.7	0	0	0	0
37	0	2.51	0	0	0	0.3
38	0	2.81	0	0	0	1.1
39	0	4.63	0	2	0	10.61
40	0	1.28	0	0	0	1.2
41	0	2.78	0	1	0	21.52

Table A1
(Continued)

Comparison of Ketone Mass Spectra (Normalized Intensities)						
Carbonyl Type Compound	Ketones					
	Acetone		2-Butanone		2-Hexanone	
42	0	9.61	0	3	0	6.61
43	100	100	100	100	78.8	100
44	0	2.46	0	3	0	2.5
45	0	0	19.15	0	100	0.8
48	0	0	0	0	0	0
49	0	0	0	0	0	0.1
50	18.91	0	10.12	0	0	1.1
51	0	0	0	0	0	1.3
52	0	0	0	0	0	0.4
53	0	0	0	0	0	1.8
54	0	0	0	0	0	0.4
55	0	0	0	0	0	3.6
56	0	0	0	0	0	1.3
57	0	0.47	0	8	0	26.32
58	0	24.84	9.03	0	0	66.47
59	0	0.93	0	0	0	4
60	50.5	0	0	0	0	0.2
62	0	0	0	0	0	0.1
63	0	0	0	0	0	0.1
65	0	0	0	0	0	0.1
67	0	0	0	0	0	0.3
69	0	0	0	0	0	0.1
71	0	0	8.73	1	0	8.41
72	0	0	0	25	0	1.5
73	0	0	0	1	0	0
74	0	0	17.74	0	0	0
78	0	0	0	0	0	0
83	0	0	0	0	48.19	0.1
85	0	0	0	0	0	11.91
86	0	0	0	0	0	0.6
96	0	0	0	0	0	0
100	0	0	0	0	0	16.11
101	0	0	0	0	0	1.4
141	0	0	0	0	0	0
143	0	0	8.68	0	0	0
159	0	0	0	0	11.97	0

Note. The relative intensity threshold of $\geqslant 0.003$ was set for LILBID, whereas in the case of NIST, all values with no threshold or exclusion are presented.

Table A2
The Mass Lines and Normalized Intensities of Aldehydes, i.e., Propanal, Butanal, and Hexanal, Are Presented Here at Combined DTs without Water Clusters

Comparison of Aldehyde Mass Spectra (Normalized Relative Intensities)						
Carbonyl Type Compound	Aldehydes					
	Propanal		Butanal		Hexanal	
Chemical formula	CH_3CH_2CHO		$CH_3(CH_2)_2CHO$		$CH_3(CH_2)_4CHO$	
Carbons	3		4		6	
Mol. weight	58		72		100	
Library	LILBID	NIST	LILBID	NIST	LILBID	NIST
m/z						
12	0	0.1	0	0.1	0	0
13	0	0.3	0	0.3	0	0
14	0	1	0	1.6	0	0.3
15	0	2.2	0	5.4	0	2.19
16	0	0.1	0	0.2	0	0
17	0	0	0	0.3	0	0.2
18	0	0	0	1.5	0	0.99
19	0	0.1	0	0.2	0	0.2
20	0	0	0	0.1	0	0
24	0	0.4	0	0.1	0	0
25	0	2.2	0	0.6	0	0
26	0	15.9	0	6.31	0	2.69
27	0	47.3	0	58.96	0	33.89
28	0	57.8	0	14.91	0	8.09
29	0	88.1	12.07	53.86	10.43	32.99
30	0	5.2	0	1.2	0	1.59
31	30.41	2.9	0	2.8	0	1.79
32	0	0	0	0	0	0.3
36	0	0.8	0	0.3	0	0
37	0	3.6	0	2.7	0	0.7
38	0	4	0	4.6	0	1.89
39	0	7	0	23.12	0	20.09
40	0	1.8	0	3	0	3.79
41	0	2.3	0	60.56	0	69.1
42	0	5.4	0	11.91	0	10.79
43	100	2.5	100	78.68	23.6	55.1
44	0	0.1	11.07	100	100	100
45	0	0	28.15	3.5	10.97	19.49
46	0	0	0	0.4	0	0.6
48	0	0	0	0.1	0	0
49	0	0	0	0.5	0	0.2
50	0	0	0	1.2	0	0.99
51	0	0	0	0.8	0	1.29
52	0	0.5	0	0.2	0	0.3
53	0	2.2	0	2.5	0	2.89
54	0	0.4	0	2.3	0	2.29
55	0	3.5	0	3	0	15.29
56	0	0.5	7.77	0.4	6.33	82

Table A2
(Continued)

Comparison of Aldehyde Mass Spectra (Normalized Relative Intensities)						
Carbonyl Type Compound	Aldehydes					
	Propanal		Butanal		Hexanal	
57	0	29.7	0	25.82	0	38.09
58	0	100	0	1.1	0	8.99
59	0	4	0	0.1	0	0.7
60	0	0.3	0	1	0	3.59
61	0	0	0	0	0	0.4
62	0	0	0	0	0	0.2
63	0	0	0	0	0	0.3
65	0	0	0	0	0	0.4
66	0	0	0	0	0	0.1
67	0	0	0	0	0	8.09
68	0	0	0	0.1	0	0.5
69	0	0	0	0.6	0	1.39
70	0	0	0	0.2	0	0.6
71	0	0	0	7.21	0	6.69
72	0	0	0	73.48	0	16.69
73	0	0	0	4.7	0	1.79
74	0	0	0	0.3	0	0.3
75	0	0	0	0.1	0	0
76	0	0	0	0	0	0
77	0	0	0	0	0	0.1
78	0	0	0	0	0	0
79	0	0	0	0	0	0.2
81	6.78	0	0	0	0	1.19
82	0	0	0	0	0	12.79
83	0	0	0	0	86.94	0.99
84	0	0	0	0	6.37	0.1
85	0	0	0	0	0	0.3
87	0	0	0	0	0	0.4
99	0	0	0	0	0	0.3
100	0	0	0	0	0	0.4
102	0	0	0	0	0	0
157	5.9	0	0	0	0	0
171	0	0	0	0	0	0

Note. The relative intensity threshold of $\geqslant 0.003$ was set for LILBID, whereas in the case of NIST, all values with no threshold or exclusion are presented.

Table A3
Organic Cationic Species that Could Potentially Coincide with Three Major Types of Water Clusters in LILBID Spectra

Major Types of Water Clusters	Coincident Organic Species		
	Acetone/Propanal	Butanone/Butanal	Hexanone/Hexanal
$[H_3O]^+(H_2O)_{n=1,2...}$	$[C_3H_3O]^+$	$[C_4H_7]^+$, $[C_3H_3O]^+$, $[C_4H_9O]^+$	$[C_4H_7]^+$, $[C_3H_3O]^+$, $[C_4H_9O]^+$
$[Na]^+(H_2O)_{n=1,2...}$	$[C_3H_5]^+$, $[C_2HO]^+$, $[C_3H_7O]^+$	$[C_3H_5]^+$, $[C_2HO]^+$, $[C_3H_7O]^+$, $[C_4H_{11}]^+$	$[C_3H_5]^+$, $[C_2HO]^+$, $[C_3H_7O]^+$, $[C_4H_{11}]^+$
$[K]^+(H_2O)_{n=0,1,2...}$	$[C_3H_3]^+$	$[C_3H_3]^+$, $[C_4H_{11}O]^+$	$[C_3H_3]^+$, $[C_4H_{11}O]^+$

A.3. Comparison of Peak Ratio

For LILBID data, the peak ratio was calculated for each ketone and aldehyde by adding the relative intensity values of 44 and 45 u peaks and dividing by the 43 u peak $(44 + 45/43)$ for the combined DT spectral data (Figure A7). A positive correlation was observed for the carbon number in carbonyl compounds and the respective peak ratios.

ORCID iDs

Nozair Khawaja https://orcid.org/0000-0001-8237-1523
Fabian Klenner https://orcid.org/0000-0002-5744-1718
Frank Postberg https://orcid.org/0000-0002-5862-4276

References

Altobeli, N., Postberg, F., Fiege, K., et al. 2016, Sci, 352, 312
Auer, A., & Sitte, K. 1968, E&PSL, 4, 178
Balsiger, H., Altwegg, K., Bochsler, P., et al. 2007, SSRv, 128, 745
Barabash, S., Wurz, P., Brandt, P., et al. 2013, EPSC, 8, 709
Belousov, A., Miller, M., Continetti, R., et al. 2021, JASMS, 32, 1162
Berg, O. E., & Richardson, F. F. 1969, RScI, 40, 1333
Brockwell, T. G., Meech, K. J., Pickens, K., et al. 2016, in IEEE Aerospace Conf. (Piscataway, NJ: IEEE), 1
Burchell, M. J., Cole, M. J., McDonnell, J. A. M., et al. 1999, MeScT, 10, 41
Cable, M. L., Porco, C., Glein, C. R., et al. 2021, PSJ, 2, 132
Charvat, A., & Abel, B. 2007, PCCP, 9, 3335
Dietzel, H., Eichhorn, G., Fechtig, H., et al. 1973, JPhE, 6, 209
Fielding, L. A., Hillier, J. K., Burchell, M. J., & Armes, S. P. 2015, ChCom, 51, 16886
Friichtenicht, J. F. 1964, NucIM, 28, 70
Friichtenicht, J. F., Roy, N. L., & Becker, D. G. 1971, in IAU Coll. 13, Evolutionary and Physical Properties of Meteoroids (Cambridge: Cambridge Univ. Press), 299
Goesmann, F., Rosenbauer, H., Roll, R., et al. 2007, SSRv, 128, 257
Grün, E., Krüger, H., & Srama, R. 2019, SSRv, 215, 46
Hillier, J. K., Green, S. F., McBride, N., et al. 2007, MNRAS, 377, 1588
Hillier, J. K., Postberg, F., Sestak, S., et al. 2012, JGRE, 117, E00902
Hillier, J. K., Sestak, S., Green, S. F., et al. 2009, P&SS, 57, 2081
Hillier, J. K., Sternovsky, Z., Armes, S. P., et al. 2014, P&SS, 97, 9
Hillier, J. K., Sternovsky, Z., Kempf, S., et al. 2018, P&SS, 156, 96
Hoffmann, J. 2010, PhD thesis, Goethe Universität Frankfurt, http://publikationen.ub.uni-frankfurt.de/frontdoor/index/index/year/2011/docId/21831
Howell, S. M., & Pappalardo, R. T. 2020, NatCo, 11, 1311
Iess, L., Stevenson, D. J., Parisi, M., et al. 2014, Sci, 344, 78
Kempf, S., Altobelli, N., Briois, C., et al. 2014, EPSC, 9, 229
Khawaja, N., Postberg, F., Hillier, J., et al. 2019, MNRAS, 489, 5231
Kissel, J., Altwegg, K., Clark, B. C., et al. 2007, SSRv, 128, 823
Kissel, J., Brownlee, D. E., Büchler, K., et al. 1986, Natur, 321, 336
Klenner, F., Postberg, F., Hillier, J., et al. 2019, RCMS, 33, 1751
Klenner, F., Postberg, F., Hillier, J., et al. 2020a, AsBio, 20, 179
Klenner, F., Postberg, F., Hillier, J., et al. 2020b, AsBio, 20, 1168
Klenner, F., Umair, M., Walter, S. H. G., et al. 2022, E&SS, 9, e02313
Ligterink, N. F. W., Grimaudo, V., Moreno-García, P., et al. 2020, NatSR, 10, 9641
Mahaffy, P. R., Webster, C. R., Cabane, M., et al. 2012, SSRv, 170, 401
Mamyrin, B. A. 1994, IJMSp, 131, 1
McComas, D. J., Christian, E. R., Schwadron, N. A., et al. 2018, SSRv, 214, 116
McLafferty, F. W., & Turecek, F. 1993, Interpretation of Mass Spectra (4th ed.; Sausalito, CA: Univ. Science Books)
Meyer, S., Tulej, M., & Wurz, P. 2017, GI, 6, 1
Miller, M. E. C., Burker, S. E., & Continetti, R. E. 2022, ESC, 6, 1813
Mocker, A., Bugiel, S., Auer, S., et al. 2011, RScI, 82, 9095111
Morse, A. D., Andrews, D. J., Morgan, G. H., et al. 2016, AcAau, 125, 196
Postberg, F., Kempf, S., Hillier, J. K., et al. 2009a, Icar, 193, 438
Postberg, F., Kempf, S., Schmidt, J., et al. 2009b, Natur, 459, 1098
Postberg, F., Khawaja, N., Abel, B., et al. 2018, Natur, 558, 564
Postberg, F., Schmidt, J., Hillier, J., et al. 2011, Natur, 474, 620
Sephton, M. A., Waite, J. H., & Brockwell, T. G. 2018, AsBio, 18, 843
Smith, R. M. 2004, in Understanding Mass Spectra: A Basic Approach, ed. R. M. Smith (2nd ed.; New York: Wiley)
Srama, R., Ahrens, T. J., Altobelli, N., et al. 2004, SSRv, 114, 465
Srama, R., Kempf, S., Moragas-Klostermeyer, G., et al. 2011, CEAS, 2, 3
Srama, R., Kobayashi, M., Krüger, H., et al. 2019, EGUGA, 21, 9105
Stevenson, D. P. 1951, FaDi, 10, 35
Thomas, P. C., Tajeddine, R., Tiscareno, M. S., et al. 2016, Icar, 264, 37
Waite, J. H., Lewis, W. S., Kasprzak, W. T., et al. 2004, SSRv, 114, 113
Wiederschein, F., Vöhringer-Martinez, E., Beinsen, A., et al. 2015, PCCP, 17, 6858